BARC/2009/E/011

DEVELOPMENT OF RESONANCE-ENHANCED MULTIPHOTON IONIZATION SYSTEM

by

P.D. Naik, Hari P. Upadhyaya, Awadhesh Kumar and P.N. Bajaj
Radiation and Photochemistry Division
and
A.K. Sinha, S. Bhatt and M.D.P. Gupta
Centre for Design & Manufacture

2009

BARC/2009/E/011

BARC/2009/E/011

GOVERNMENT OF INDIA
ATOMIC ENERGY COMMISSION

DEVELOPMENT OF RESONANCE-ENHANCED MULTIPHOTON IONIZATION SYSTEM

by

P.D. Naik, Hari P. Upadhyaya, Awadhesh Kumar and P.N. Bajaj
Radiation and Photochemistry Division
and
A.K. Sinha, S. Bhatt and M.D.P. Gupta
Centre for Design & Manufacture

BHABHA ATOMIC RESEARCH CENTRE
MUMBAI, INDIA
2009

BIBLIOGRAPHIC DESCRIPTION SHEET FOR TECHNICAL REPORT
(as per IS : 9400 - 1980)

01	*Security classification :*	Unclassified
02	*Distribution :*	External
03	*Report status :*	New
04	*Series :*	BARC External
05	*Report type :*	Technical Report
06	*Report No. :*	BARC/2009/E/011
07	*Part No. or Volume No. :*	
08	*Contract No. :*	
10	*Title and subtitle :*	Development of resonance-enhanced multiphoton ionization system
11	*Collation :*	56 p., 19 figs., 8 tabs., ills.
13	*Project No. :*	
20	*Personal author(s) :*	1) P.D. Naik; Hari P. Upadhyaya; Awadhesh Kumar, P.N. Bajaj 2) A.K. Sinha; S. Bhatt; M.D.P. Gupta
21	*Affiliation of author(s) :*	1) Radiation and Photochemistry Division, Bhabha Atomic Research Centre, Mumbai 2) Centre for Design and Manufacture, Bhabha Atomic Research Centre, Mumbai
22	Corporate author(s) :	Bhabha Atomic Research Centre, Mumbai-400 085
23	*Originating unit :*	Radiation and Photochemistry Division, BARC, Mumbai
24	*Sponsor(s) Name :* *Type :*	Department of Atomic Energy Government

Contd...

30	*Date of submission :*	April 2009
31	*Publication/Issue date :*	May 2009
40	*Publisher/Distributor :*	Associate Director, Knowledge Management Group and Head, Scientific Information Resource Division, Bhabha Atomic Research Centre, Mumbai
42	*Form of distribution :*	Hard copy
50	*Language of text :*	English
51	*Language of summary :*	English, Hindi
52	*No. of references :*	20 refs.
53	*Gives data on :*	
60	*Abstract :* Radiation and Photochemistry Division has developed a Molecular Beam-Resonance Enhanced Multiphoton Ionization-Time-of-Flight spectrometer, a highly sensitive and selective analytical detection system, for investigation of photodissociation dynamics of isolated molecules. In this system, the molecular beam is intersected in the extraction region of a Wiley-McLaren type Time-of-Flight mass spectrometer by the photolysis laser beam, propagating perpendicular to both the molecular beams and the Time-of-Flight tube. The probe (ionization) laser beam counter propagating to the photolysis beam, ionizes the stable products and the radicals produced on photodissociation. The important features of the system, namely, the resolution and the detection limit, have been determined from the studies of aniline molecular beam, generated by seeding 1% aniline in helium. For the present configuration, using one metre long flight tube, the resolution has been found to be about 400, and detection limit is better than 10^6 species per cm^3. The integrity of the set-up is obtained from the photodissociation dynamics studies of bromoform.	
70	*Keywords/Descriptors :* IONIZATION CHAMBERS; MOLECULAR BEAMS; HYDRODYNAMICS; TIME-OF-FLIGHT MASS SPECTROMETERS; LASER RADIATION; MULTI-PHOTON PROCESSES; SPECIFICATIONS; EXCIMER LASERS; NEODYMIUM LASERS	
71	*INIS Subject Category :*	S46
99	*Supplementary elements :*	

CONTENTS

FIGURES, DRAWINGS AND PICTURES

FIGURES

DRAWINGS

PICTURES

TABLES

ABSTRACT

Radiation & Photochemistry Division has developed a Molecular Beam-Resonance Enhanced Multiphoton Ionization-Time-of-Flight spectrometer, a highly sensitive and selective analytical detection system, for investigation of photodissociation dynamics of isolated molecules. In this system, the molecular beam is intersected in the extraction region of a Wiley-McLaren type Time-of-Flight mass spectrometer by the photolysis laser beam, propagating perpendicular to both the molecular beams and the Time-of-Flight tube. The probe (ionization) laser beam counter propagating to the photolysis beam, ionizes the stable products and the radicals produced on photodissociation. The important features of the system, namely, the resolution and the detection limit, have been determined from the studies of aniline molecular beam, generated by seeding 1% aniline in helium. For the present configuration, using one metre long flight tube, the resolution has been found to be about 400, and detection limit is better than 10^6 species per cm^3. The integrity of the set-up is obtained from the photodissociation dynamics studies of bromoform.

DEVELOPMENT OF RESONANCE-ENHANCED MULTIPHOTON IONIZATION SYSTEM

P. D. Naik, Hari P. Upadhyaya, Awadhesh Kumar, P.N. Bajaj
Radiation and Photochemistry Division
Bhabha Atomic Research Centre,
&
A.K. Sinha, S. Bhatt, M.D.P. Gupta
Centre for Design & Manufacture
Bhabha Atomic Research Centre, Mumbai 400 085

1. Introduction

Molecular Beam-Resonance Enhanced Multiphoton Ionization -Time-of-Flight (MB-REMPI-TOF) is a highly sophisticated analytical detection system [1], having advantages of three techniques embedded in its name. Resonance ionization is a photo-physical process in which electromagnetic radiation is used to ionize atoms, molecules, or radicals, via an excited state, prepared resonantly. In this process, the atomic, or molecular, system serves as a summing device for storing the energy of the resonantly absorbed photons, and when, on absorption of one more photon, the energy exceeds the ionization potential, this leads to spontaneous ionization. In most of the chemical species, the resonantly prepared excited state is just one-photon transition below the ionization continuum.

REMPI is designated on the basis of the number of photons employed resonantly to prepare the excited state. The REMPI process, in which one photon is used for resonant formation of the excited state, and another photon for pumping the prepared state into the ionization continuum, is designated as (1+1) REMPI (Fig.1). This process occurs when the excited state prepared by mono-photonic absorption has energy more than half of the ionization energy. The above ionization process requires relatively low laser intensities, and thus leads to the minimal fragmentation of the parent ion. The other variants commonly employed are (2+1) and (3+1) REMPI, where two and three photons, respectively, are resonant with the electronic transitions of an atom, or a molecule. In the above processes, the final transition is saturated at a typical intensity of about 10^{26} photons cm^2 s^{-1} obtained from nanosecond pulsed laser system.

In detection of chemical species, in gas phase at the room temperature, by the REMPI technique, only a small fraction of the total available molecules is accessible to the excitation process. This is due to broad population distribution in the ro-vibrational states, expressed by

the Boltzmann equation. Thus, in order to improve the REMPI sensitivity, and also to make the transitions sharp, the population in the ground state has to be enhanced, and collisions between the gas molecules themselves, as well as with the background gas molecules have to be minimized. Both these objectives can be realized by employing supersonic beams. Supersonic beams can provide an intense source of molecules traveling with a fixed velocity in a given direction in vacuum, having an extremely narrow velocity distribution, isolated from each other, and cooled to such an extent that the excited rotational and vibrational levels are almost depopulated [2]. The supersonic molecular beams also enable to prepare molecular reactants in well-defined quantum states, with known translational energy. Thus, supersonic beams can be employed for carrying out quantum-state-selective chemistry, as well as to investigate the effect of translational energy on the reaction cross-section.

Radiation & Photochemistry Division has previously developed, and extensively employed, the Laser Photolysis-Laser induced Fluorescence (LP-LIF) technique for investigation of gas-phase reaction dynamics [3-7]. REMPI, being ionization based detection technique, is much more sensitive, versatile and can be applied to systems not amenable by LIF. The development of MB-REMPI-TOFMS system was undertaken to augment the present infrastructure, to carry out studies on photodissociation dynamics of a variety of molecules. In a photodissociation experiment, employing MB-REMPI-TOFMS system, the molecular beam is intersected in the extraction region of a Wiley-McLaren type TOF mass spectrometer [8] by the photolysis laser beam, propagating perpendicular to both the molecular beams and TOFMS. The probe (ionization) laser beam, counter propagating to photolysis beam, ionizes the stable products and the radicals produced on photodissociation, and are analyzed by TOFMS.

Since hydrodynamic cooling is an important aspect of the system that we have developed, we shall first describe hydrodynamic cooling, the means to achieve this and broad areas of applications. This will be followed by description of the development of MB-TOFMS, control and electronic system, system alignment, standardization and calibration, and finally, photodissociation of $CHBr_3$, to demonstrate the capability of the developed system.

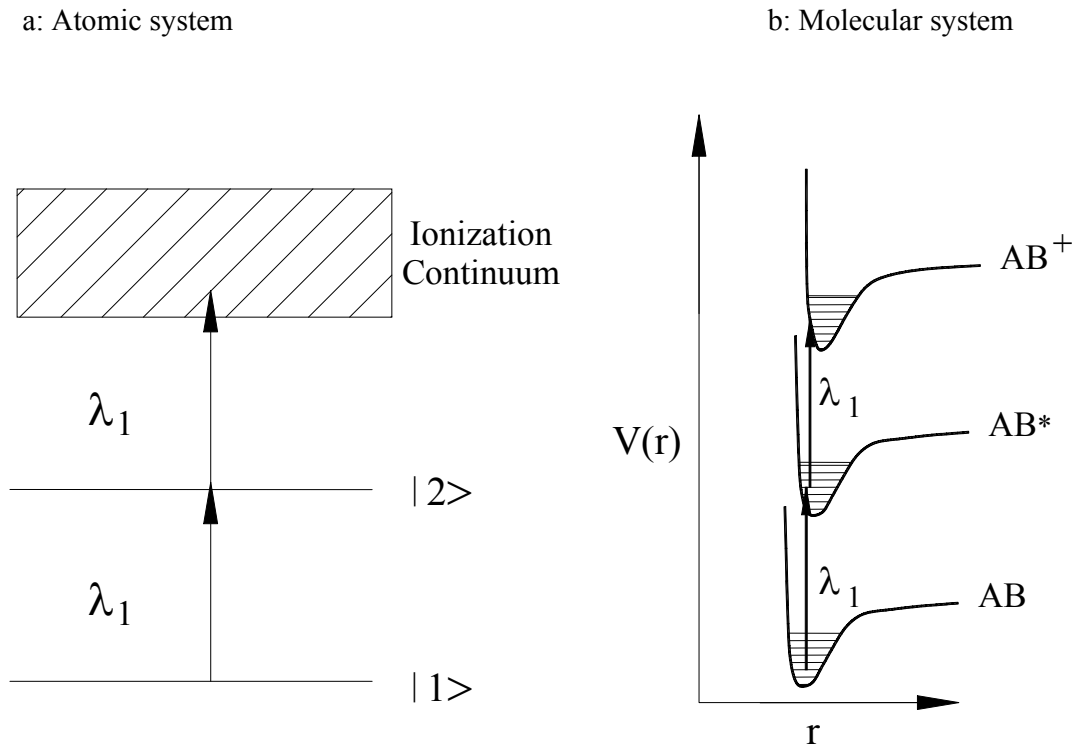

Fig 1: Schematic of 1+1REMPI processes in atomic (a) and molecular (b) systems

2. Hydrodynamic Cooling

In hydrodynamic expansion, gas, or vapour, of interest, either by itself, or in a carrier gas of low mass and high specific heat ratio *(γ)*, is discharged from a reservoir at high pressure through a nozzle, or an orifice, into an expansion chamber, maintained at low pressure by vacuum pumps of adequate speeds. Oil diffusion and roots blower pumps are commonly used to pump down the expansion chamber. The collisions constitute the heart of the hydrodynamic expansion and the concomitant cooling. The requisite parameter to obtain hydrodynamic flow is that the source Knudsen number (K_n), $K_n = \lambda/D$, is far less than unity ($K_n << 1$), where λ is the mean free path and D is the characteristic dimension (diameter or width of the nozzle). The above condition ensures sufficient collisions during expansion, and thus, during the expansion, the random thermal energy of the gas, or the vapour, gets converted into directed kinetic energy of the flow through elastic collisions, resulting in a very low temperature.

In a supersonic source, the flow velocity is very high, which results in a short flow time compared to diffusion time, leading to a non-equilibrium process. Under such condition, the expanding gas may be considered as ideal, for which viscous and heat conduction effects may be neglected. The application of conservation of energy, before and after expansion of the gas through a nozzle, results in the relation,

$$H_o = H + \frac{1}{2}mu^2 \qquad (1)$$

where, H_0 and H are the enthalpies of the gas in the stagnation chamber and the flow field, respectively, and u is the flow velocity, after expansion of the gas molecules through the nozzle. As the gas expands, and gets cooled, the enthalpy of the gas decreases, and the flow velocity increases. Thus, a large flow velocity is generated at the cost of the internal energy of the expanding species.

For an ideal gas, $H=c_pT$. The energy balance equation (1) becomes

$$c_pT_o = c_pT + \frac{1}{2}mu^2 \qquad (2)$$

where T_o is the stagnation temperature and T is the local temperature in the flow field of the jet, as measured by a thermometer being carried along the expansion streams at velocity u.

Using the expressions of the local sound velocity, $a = (\gamma kT/m)^{1/2}$, the heat capacity difference, $c_p-c_v=k$, and the specific heat ratio, $\gamma=c_p/c_v$, of the expanding gas,

or vapour, eqn. (2) can be expressed as

$$u = \left[\frac{\gamma}{\gamma - 1} \frac{2kT}{m} \left(T_o - T \right) \right] \tag{3}$$

In terms of Mach number, defined as the ratio of the flow velocity (u) to the local sound velocity (a), i.e., M=u/a, eqn.(3) can be expressed as,

$$\frac{T}{T_o} = \left[1 + \frac{\gamma - 1}{2} M^2 \right]^{-1} \tag{4}$$

Mach number is a measure of cooling/degree of expansion. Flow at any point is subsonic, sonic, or supersonic, depending on whether $M < 1$, $= 1$, or > 1. The flow through a Laval nozzle is sonic at the throat of the nozzle, and the shape of the diverging section governs the downstream flow. The rate of expansion is governed by the rate of change of the cross-sectional area. As Mach number increases, the flow velocity increases, but, at higher Mach number, the increase in Mach number is due to decrease in sound velocity as a result of decrease in temperature. Translational temperature as low as 0.015 K (for T_o = 300 K) has been achieved by this technique [9].

In terms of pressure, density, or number density, the eqn. (4) can be expressed as

$$\frac{T}{T_o} = \left(\frac{P}{P_o} \right)^{\frac{\gamma-1}{\gamma}} = \left(\frac{\rho}{\rho_0} \right)^{\gamma-1} = \left(\frac{n}{n_0} \right)^{\gamma-1} = \left[1 + \frac{\gamma - 1}{2} M^2 \right]^{-1} \tag{5}$$

where P_o and n_o are the stagnation pressure and number density, respectively; P and n are the corresponding parameters in the hydrodynamic flow field.

At the throat of the nozzle, M=1, and, therefore, the corresponding temperature, T^*, pressure, P^*, density, ρ^*, or number density, n^*, are

$$\frac{T^*}{T_0} = \frac{2}{\gamma + 1} \tag{6}$$

$$\frac{\rho^*}{\rho_o} == \frac{n^*}{n_o} = \left(\frac{2}{\gamma + 1} \right)^{\frac{1}{\gamma-1}} \tag{7}$$

$$\frac{P^*}{P_0} = \left(\frac{2}{\gamma+1}\right)^{\frac{\gamma}{\gamma-1}} \tag{8}$$

Once Mach number is known, all the other thermodynamic parameters can be calculated.

2.1 Free-jet Expansion

The flow through a converging nozzle, or an orifice, into vacuum, or a low pressure region, is sonic at the nozzle exit. Such a flow is under-expanded. It would further expand free of the containing nozzle walls, and is, therefore, called free-jet. Most of the workers using hydrodynamic sources have done away with the diverging supersonic section of the Laval nozzle because of fabricational and operational problems.

The axial Mach number in a free-jet from a converging nozzle, or circular orifice, is given by [10].

$$M = A(\gamma)\left(\frac{X - X_o}{D}\right)^{\gamma-1} - \frac{\frac{1}{2}\frac{\gamma+1}{\gamma-1}}{A(\gamma)\left(\frac{X - X_o}{D}\right)^{\gamma-1}} \tag{9}$$

where X/D is the reduced distance downstream of the nozzle, and A(γ) and X_o are constants, the values of which are given in Table 1.

For X/D >> 4,

$$M = A(\gamma)\left(\frac{X}{D}\right)^{\gamma-1} \tag{10}$$

According to eqn. (9), or (10), Mach number increases with distance, and knowing Mach number at any location, one can predict temperature and other charateristics. But, the simple picture developed so far gets blurred, to some extent, by other phenomena, such as rarefaction, shock waves and cluster formation. As the expansion progresses, the number density and temperature decrease. Consequently, the collision rate decreases, and eventually, it becomes so low that the flow becomes molecular, and all the axial flow parameters are frozen. The frozen parameters are used to derive information about the relaxation phenomena operative upstream

[11,12]. The terminal Mach number, a measure of maximum cooling under given conditions, is given by [11]

$$M_T = F(\gamma) \left(\frac{K_{n_o}}{\varepsilon} \right)^{-\left(\frac{\gamma-1}{\gamma}\right)} \tag{11}$$

where K_{n_o} is the source Knudsen number, ε is the collision effectiveness, i.e., the maximum fractional change in the mean random velocity per collision per molecule, and the expression for F(γ) is

$$F(\gamma) = 2^{\frac{3\gamma-2}{2\gamma}} \gamma \left[\{\pi\gamma(\gamma-1)\}^{\frac{\gamma-1}{\gamma}} \left\{ \frac{1}{2}(\gamma-1)^{\gamma+1} A^2(\gamma) \right\}^{\frac{1}{\gamma}} \right]^{-\frac{1}{2}}. \tag{12}$$

For monatomic gases (γ=5/3), the equation (11) reduces to

$$M_T = 2.05 \left(\frac{K_{n_o}}{\varepsilon} \right)^{-0.4}. \tag{13}$$

For argon, ε=0.25, and, therefore,

$$M_T = 1.17 \left(K_{n_o} \right)^{-0.4} = 1.17 \left(\frac{\lambda_o}{D} \right)^{-0.4}. \tag{14}$$

In terms of stagnation pressure,

$$M_T = 133 \left(P_o D \right)^{-0.4} \tag{15}$$

where P_o is in atmospheres and D is in cm.

Substituting the value of the terminal Mach number in eqns.(3) and (4), one can determine terminal velocity and temperature, respectively.

The degree of cooling in a free-jet depends on the total number of binary collisions, which, in turn, depends on the product of the stagnation pressure *(P_o)* and the nozzle or orifice diameter (D). So, very low temperature can, in principle, be achieved by using larger values of P_oD. Since the flow through a nozzle is (F)$\propto P_oD^2$, the practical limit to cooling is imposed by the pumping speed required to handle the gas discharge through the nozzle. For condensable gases, pumping speed can be augmented by cryo-pumping. However, in such cases, the nature of the gas limits the achievable Mach number. Earlier, the brute force approach of using large capacity pumps was the common trend to cope up with the high throughput required, to obtain low temperature and high number density supersonic free-jets and beams. But, now, two alternative approaches are being followed to achieve a higher degree of cooling, with a given

pumping system. These are: (i) the use of pulsed nozzle, where the gas flows only for a short time, and (ii) working at higher background pressure in the expansion chamber.

The first option permits higher peak gas loads, and hence higher degree of cooling, while maintaining the average gas load low, depending on the duty cycle. For an expansion chamber that is large enough, we can perform many interesting experiments between the time that isentropic flow is established and the time the first batch of the gas molecules is scattered from the walls of the chamber, and contributes to the background pressure. So, the pump required should be just large enough to evacuate the chamber, before the arrival of the next pulse. The pumping speed, in this case, sets a limit on the pulse repetition rate, for a given P_oD value, and does not affect the characteristics of the expansion. Such a source is well-suited for spectroscopic studies, chemical dynamics, cluster science, etc.

In the second option, high throughput required for high degree of cooling is pumped at higher pressure in the expansion chamber. But, the interaction of the free-jet with the high background pressure in the chamber results in the formation of a well-defined shock wave system that surrounds the cold isentropic core of the jet, and shields it from the warm background gas. Fig.2 shows schematic of such an expansion. Isentropic expansion region is surrounded by a barrel shock wave at the sides and Mach disc normal to the flow centerline. The shock waves reheat the gas molecules, and thus destroy all the advantageous characteristics achieved during expansion; the thickness of the shock wave is of the order of a few local mean free paths. The region between the barrel shock and the boundary is non-isentropic, whereas the inner core of the expansion remains un-perturbed, and hence called zone of silence. All the expressions derived earlier are valid in the zone of silence. This type of source is well-suited for spectroscopic studies. Optical absorption and fluorescence studies should be carried out, before the Mach disc location. The location of the Mach disc in a free-jet expansion from a circular nozzle, or an orifice, is approximately given by [13]

$$\frac{X_M}{D} = 0.66\left(\frac{P_o}{P_b}\right)^{\frac{1}{2}}. \qquad (16)$$

2.2 Internal Relaxation

The elastic collisions in a free-jet expansion result in a low translational temperature. The internal degrees of freedom of the expanding species, viz., the rotational and the

vibrational degrees of freedom of molecules and low-lying electronic levels of atomic and molecular species, communicate with the translationally cold bath through inelastic collisions, and are cooled extensively. The whole process is iterative. Since the number of collisions, a pre-requisite for equilibration, is finite for a given expansion, the final state of the system is governed by kinetics rather than thermodynamics, and would often be a non-equilibrium state. The total number of collisions that occur during the expansion depends on the product of stagnation number density and nozzle diameter, as mentioned earlier. The energy transfer cross-section is dependent on the energy difference between the energy levels, and, hence, is higher in the case of translational degrees of freedom, as compared to the rotational levels, which is higher than the vibrational levels, and this results in the following inequalities for temperatures, $T_{trans} < T_{rot} < T_{vib} < T_0$. Therefore, the study of such expansions, in itself, is of great importance, to understand the dynamics of cooling of polyatomic molecules. The hydrodynamic cooling confines the population in only a few low-lying energy levels of the molecules.

Collision-dominated low temperature bath provided by hydrodynamic expansion can foster clustering. However, as cluster formation is slower than the rotational, or even the vibrational relaxation, extensive internal cooling can be achieved, before clustering becomes significant. On the other hand, one can optimize the operational conditions, to generate significant amounts of clusters, for carrying out very interesting studies, which are currently at the forefront of the fundamental and the applied research. The advantage of hydrodynamic cooling is that it is free from perturbations and loss of information about molecular motions, unavoidable in the technique of matrix isolation.

2.3 Supersonic Beams

Kantrowitz and Grey [14] suggested, in 1951, the use of hydrodynamic flow for generating high intensity molecular beams. Since then tremendous advances have been made in the design and operation of these beam sources. A well-collimated supersonic molecular beam can be generated by skimming the core of a supersonic flow through a Laval nozzle, or a free-jet, with a hollow truncated cone, and employing additional collimators downstream of the flow. In order to generate molecular beam from a free-jet expansion in high background pressure, skimmer must be placed well before the shock front (Mach disc). According to eqn. (9), by selecting a suitable skimmer

nozzle distance, one may expect to produce a beam of any desired Mach number, and hence temperature, and predict other characteristics of the beam. But, this simple picture gets blurred, to some extent, by other phenomena, such as rarefaction, shock waves and cluster formation, as mentioned earlier.

The skimmer has a two-fold function. Firstly, it separates the expansion chamber, with high background density, from the beam chamber. For this function, the shape of the skimmer body and nozzle to skimmer distance have to be chosen to minimize the attenuation of centerline intensity due to skimmer interaction and collisions with the residual gas in the expansion chamber. Secondly, it also serves as a collimator, which defines the shape attachment of the bow shock wave to the cone apex. The shape and size are not arbitrary, but stem from a careful balance of somewhat conflicting requirements. Since it is immersed in a supersonic stream, it will give rise to a bow shock wave (cf. fig.3). Depending on the Mach number of the free stream, there is maximum included angle of the sharp pointed cone, which can result in attachment of the bow shock wave to the cone apex. If the cone angle is greater than this critical value for a particular Mach number, the shock wave will be detached, and the gas in this region will be in the thermodynamic post-shock state. Under such circumstances, all the prospective advantages of a supersonic beam will be frittered. Therefore, the cone angle must be such that the shock wave is attached. It has been found that, if the included cone angle is 60^0 or less, all the bow shock waves at Mach number above 1.5, will be attached. At higher Mach number, a slightly higher angle can be tolerated, but about 60° is a convenient design criterion, and has been widely used. Even if the shock wave is attached, there is no implicit assurance that the skimmer flow indeed will be supersonic. Since the thickness of a shock wave is a few free-stream mean free paths, the molecules of the gas passing through the shock wave must undergo at least a few collisions in passing from the free stream to the post shock state. If the diameter of the skimmer inlet is of the order of a free-stream mean free path, one can expect that when the bow shock wave is attached in macroscopic terms, the gas reaching the inlet will not have undergone enough collisions to degrade it to the post-shock conditions. If the mean free path in the free stream is much larger than the skimmer inlet diameter, the gas flowing through the skimmer into the very low pressure region may approach the free-stream condition. The minimum ratio of the free-stream mean free path to skimmer inlet diameter, i.e., the skimmer Knudsen number, necessary to avoid collisional perturbations of the free-stream state is not obvious. Skimmer diameter of the order of the free-stream mean free path is a convenient design criterion.

There can be collisional perturbation of the skimmer flow by the molecules reflected from the inner surface of the skimmer. To minimize this effect, the edge of the skimmer opening must be as sharp as possible, and the included internal angle of the skimmer cone must be as large as possible. This is limited by the expertise in fabrication. Anderson et al. [15] observed that, with smaller internal included angle, the scattering loss was more at high jet intensities. The effect of internal angle was less pronounced at low jet intensities. One can notice the contradictory requirement that, the jet density must be high, if Mach number is to be high, and low, if collisionless flow through the skimmer is to be achieved with skimmer inlet diameter of any reasonable size.

The axial number density of a supersonic beam at a distance l_b downstream from the skimmer is

$$n_{sb} = n_s A_s \left[\frac{3}{2} + \frac{1}{2} \gamma M^2 \right] \frac{1}{\pi l_b^2}. \tag{17}$$

The higher degree of directionality of a supersonic beam, as compared that of a free-jet, reduces the collision rate. Since the Doppler width of an absorption line is dramatically reduced, the supersonic beams are very useful for high resolution spectroscopy, especially of complex molecules. In view of their special characteristics, such as high degree of directionality, high number density, narrow velocity distribution, low internal temperature for polyatomic molecules, nearly collision-free environment, supersonic free-jets and beams are being increasingly used in a variety of fields, e.g., spectroscopy, chemical dynamics, gas dynamic lasers, isotope separation, cluster science, surface science, etc.

3. MB-REMPI TOFMS System

The integrated system is shown schematically in Fig. 4, and drawing D1 shows the mechanical drawing. The photograph P1 is the picture of the assembled set-up. The MB-REMPI-TOFMS system consists of differentially-pumped two vacuum chambers, the expansion chamber and the ionization/detector chamber. The expansion chamber houses the pulsed nozzle-skimmer assembly, and the average load in this chamber is ~ 1.4 torr lit per sec, for a typical stagnation pressure of 1 atmosphere, nozzle dia. 0.08 cm, pulse width 100 μs and repetition rate of 20 Hz. The mass flow rate (F) was obtained from the expression F= n*u*A, where n*, u* and A are number density, flow velocity at the nozzle throat and the diameter of the nozzle, respectively. At the throat of the nozzle, Mach no., M=1, hence,

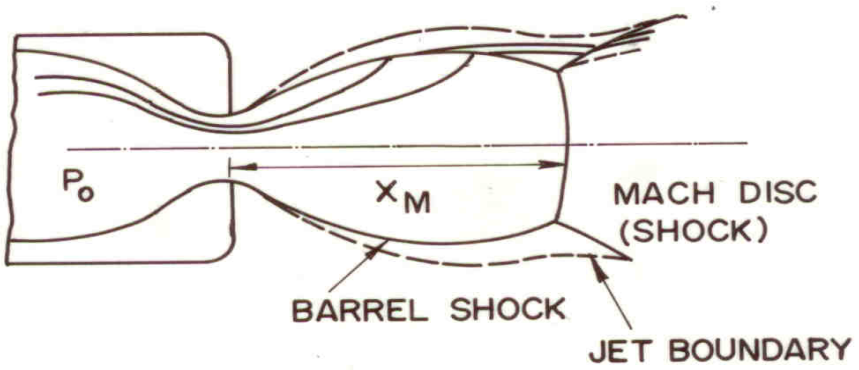

Fig.2: Schematic of free-jet expansion.

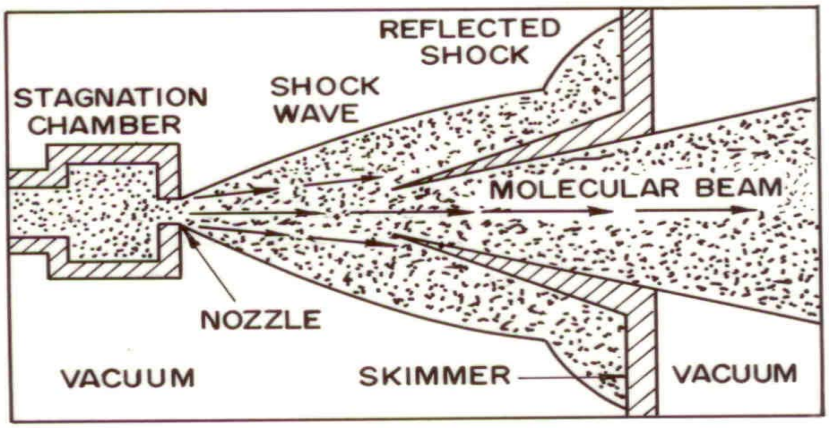

Fig.3: Free-jet-skimmer interface.

the flow velocity, $u^*=a=(\gamma kT^*/m)^{1/2}$. T* and n* are evaluated from the eqns. 6 and 7, respectively. In order to increase the axial distance of Mach disk occurrence from the nozzle exit, i.e., to obtain the highest mach no., vacuum of ~ 10^{-4} torr is required, and the same was obtained by a turbo molecular pump (900 l/s, Alcatel, France). The load in the ionization chamber is $8x10^{-6}$ torr lit per sec, for a typical nozzle skimmer distance of 20 mm and skimmer dia. of 2 mm. This chamber houses TOFMS and fly-through fast ionization gauge, and is pumped by a turbo-molecular pump of speed 400 l/s (Elettrorava, Italy). The time-of-flight tube, which is attached to the ionization chamber, is pumped by another turbo-molecular pump of speed 250 l/s (Pfiffer, Germany) to obtain a vacuum of ~ 10^{-8} torr, in the detector region. All the turbo pumps are backed by rotary pumps (Alcatel model). The detector chamber has provision for LIF detection also.

The vacuum system was fabricated in CDM, BARC. It was tested for any vacuum leak, using a He-leak detector. The vacuum system was baked and pumped for a week, to degas the inner surface of the chambers and other accessories inside the chambers. The dynamic vacuum, in the absence of any gas load, was found to be better than 10^{-6} torr in all the chambers.

3.1 Expansion Chamber

The expansion chamber is made from a cylindrical stainless steel tube of OD=256 mm, with wall thickness of 3.5 mm. The chamber has two big-ports, for details, see drawing D2. One of the big ports is used for connecting turbo molecular pump via DN 200 connection, and the other for accessing and working inside the chamber. The above two ports are attached on the opposite sides at the middle of the chamber. In addition, the chamber has four DN-40 ports, with cover conflate flanges of dia. 70 mm. The nozzle-skimmer assembly is mounted on the end-flange, on the side of the ionization chamber, see drawing D3 for details.

The flange, with ¼ ″ stainless steel tube welded at its centre, is mounted on the end flange at the free-end side of the expansion chamber. The outside end of the ¼ ″ tube is connected to the gas reservoir, while the inside end is connected to the ¼ ″ tube of the pulsed valve (nozzle). For detailed information, refer to the drawing D4.

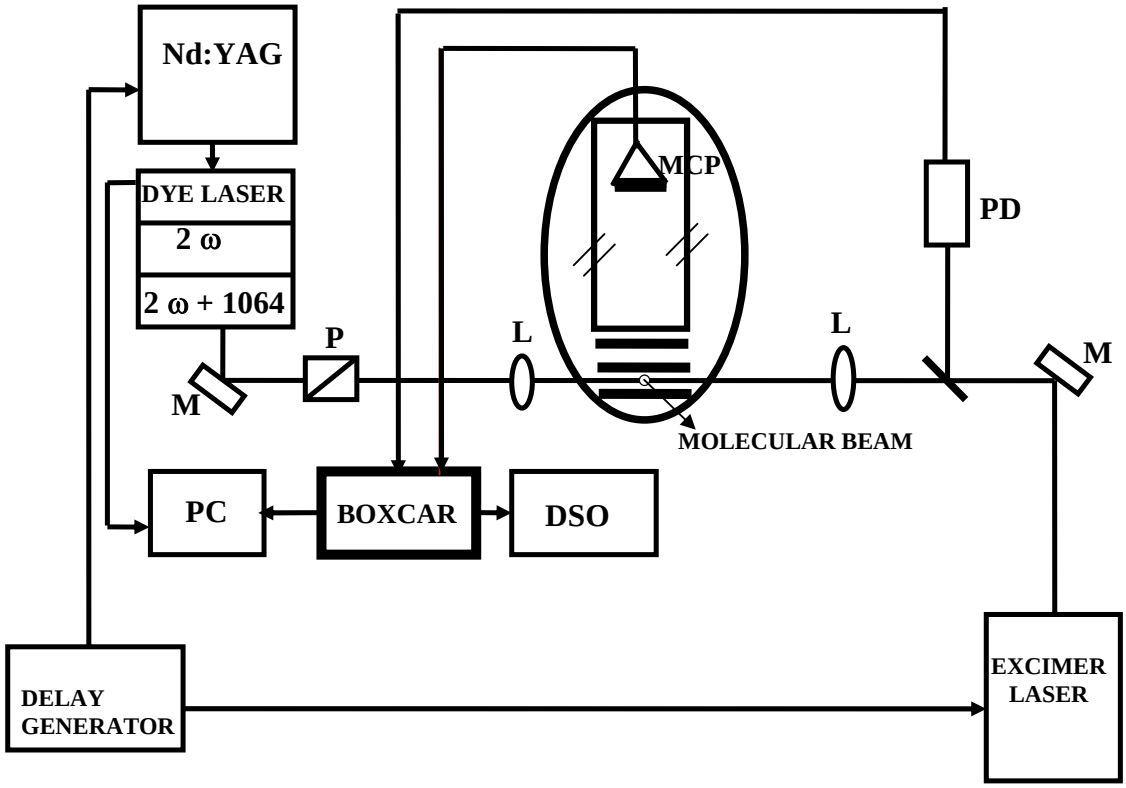

Fig.4: Schematic of the probe laser system and control electronics.

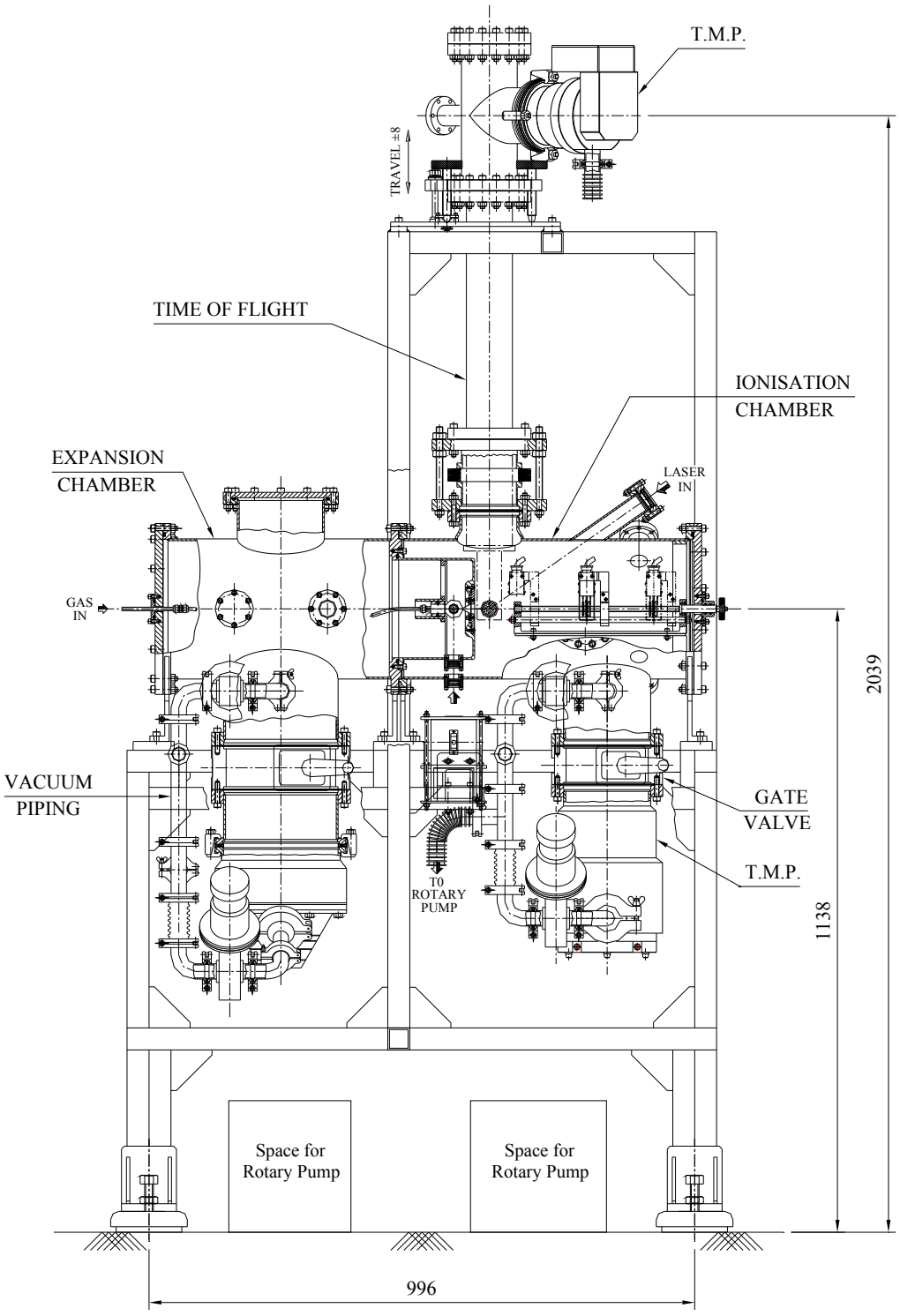

DRAWING D1 : INTEGRATED DRAWING OF MB-REMPI-TOF

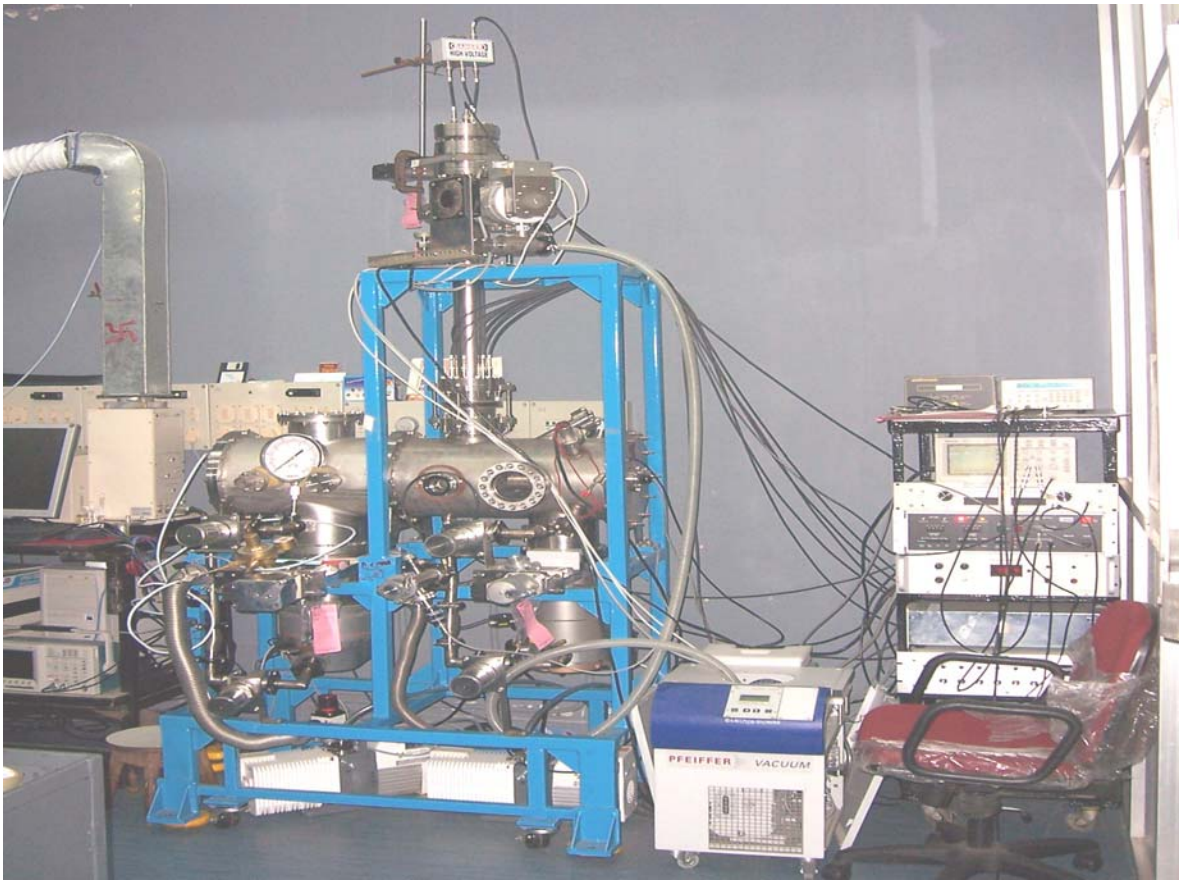

Photograph P1: A picture of the MB-REMPI-TOFMS system

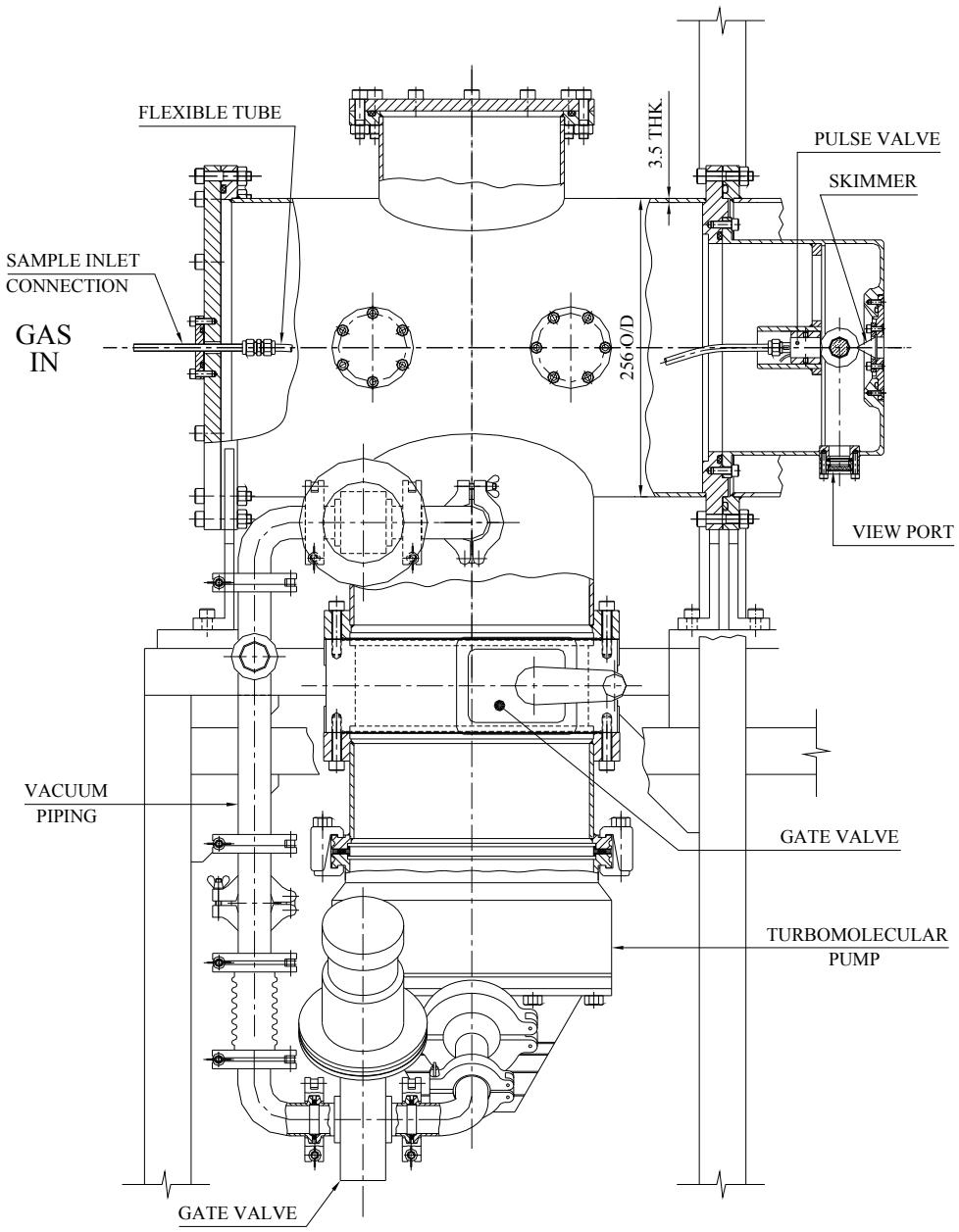

DRAWING D2 : EXPANSION CHAMBER WITH PUMP OF MB-REMPI-TOF

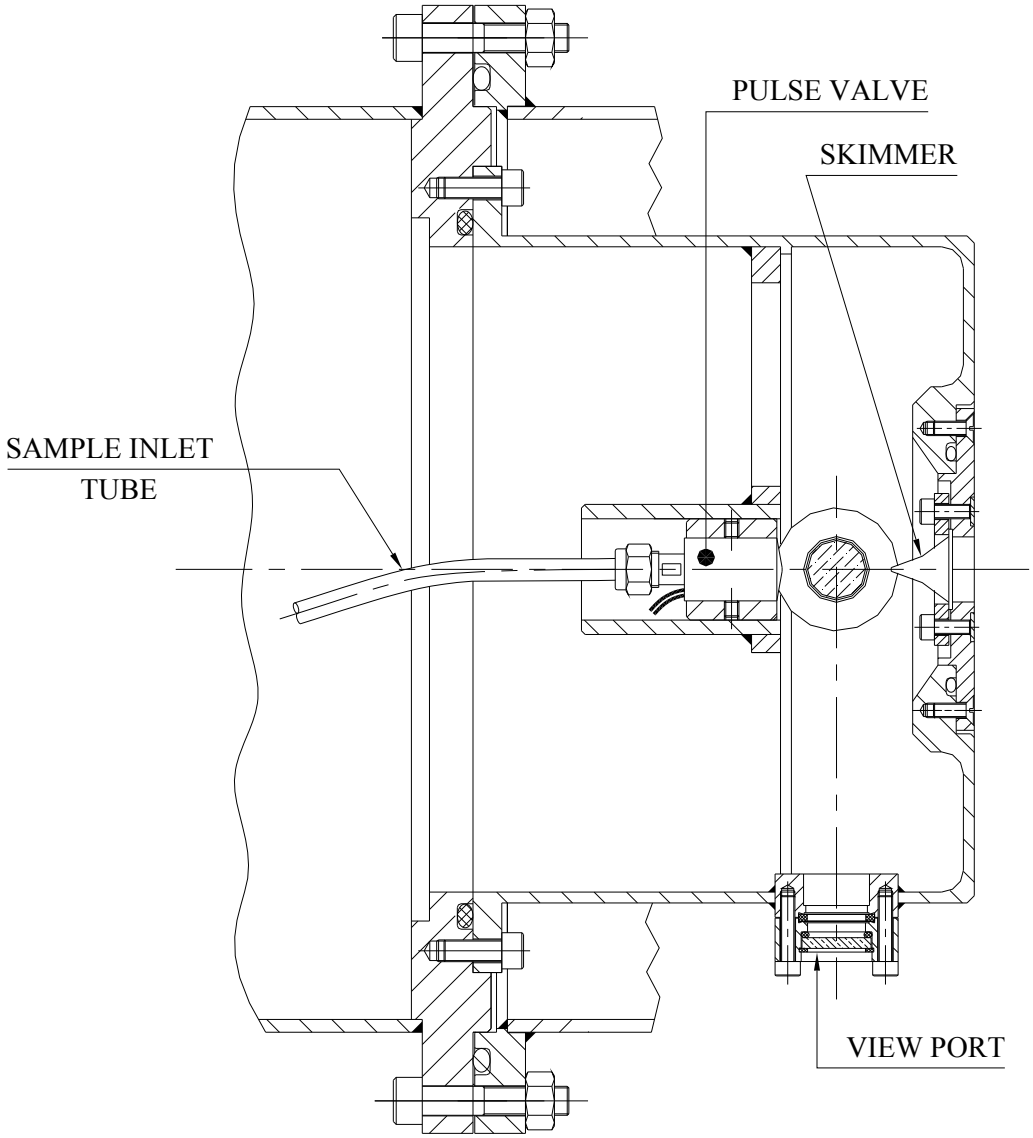

DRAWING D3 : NOZZLE SKIMMER ASSY. OF MB-REMPI-TOF

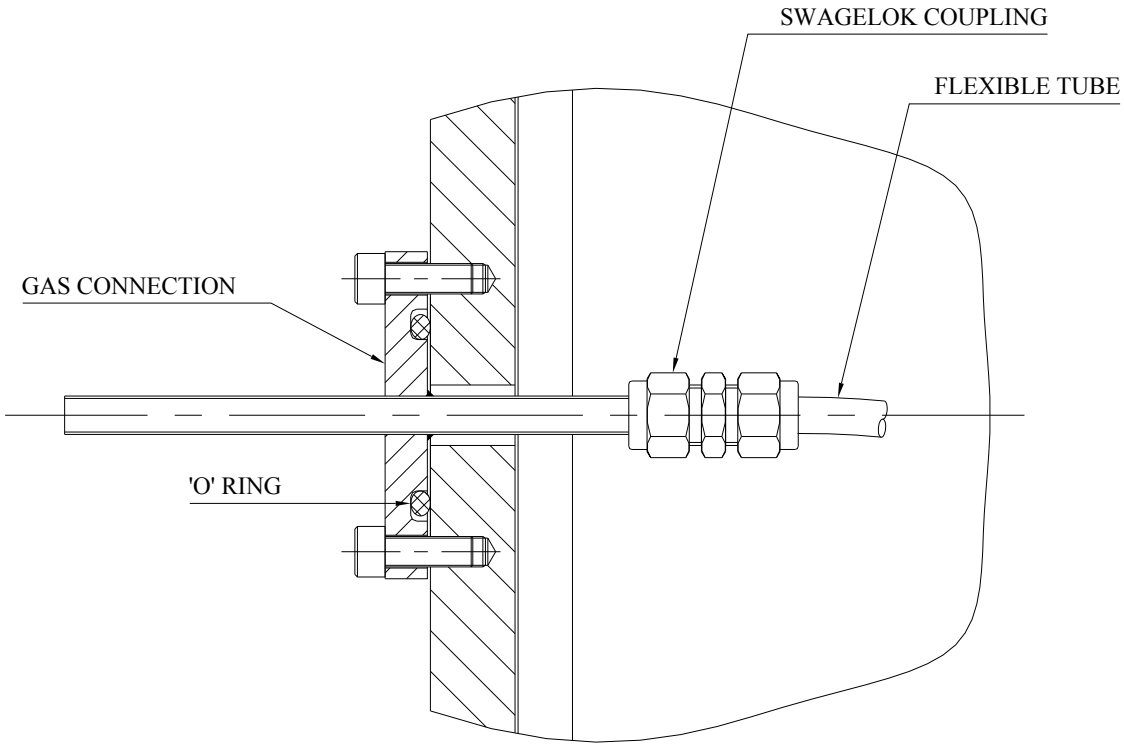

DRAWING D4 : TUBE CONNECTION FOR SAMPLE INLET

Table 1: Values of the constants for eqn. (9).

γ	X_0/D	$A(\gamma)$	M
1.67	0.075	3.26	
1.40	0.40	3.65	
1.30	0.70	3.90	
1.2857	0.85	3.96	
1.20	1.0	4.29	
1.10	1.60	5.25	
1.05	1.80	6.44	

Table 2(a): Specifications of the pulsed nozzle valve and the controller.

S.No.	Feature	Specification
1.	Orifice diameter	0.8 mm (variable)
2.	Pulse duration	100 μs minimum (variable)
3.	Repetition rate	0-50 Hz
4.	Operating pressures	Vacuum to 1000 psi

Table 2(b): Specifications of Molecular Beam Skimmer.

S.No.	Feature	Specification
1.	Orifice diameter	2 mm
2.	Length to apex	0.75" (1.92 cm)
3.	Base diameter	0.9" (2.29cm)
4.	Total included angle at base	50°
5.	Material	Nickel
6.	Finish	Base flange is ground finish and polished to seal without soldering

Table 2(c): The typical characteristic features of the nozzle-skimmer assembly.

	Nozzle-Skimmer Assembly	Characteristics
1	Pulse width	500 ms
2	Distance between nozzle to skimmer	20 mm
3	Distance between nozzle to laser beam interaction region	75 mm

3.2 Nozzle-Skimmer Assembly (Molecular Beam Source)

In order to reduce the population of the higher internal states of the dissociating molecules, we have prepared the supersonic molecular beam of chemical species of interest by hydrodynamic expansion of the molecules seeded in a buffer gas, such as helium or argon, through a nozzle, and skimming the free-jet thus formed. The dynamic cooling in supersonic expansion avoids the perturbation and spectral broadening inherent in conventional static cooling, and, at the same time, retains the super-cooled molecules in the gas phase in sufficient density. In the present system, a solenoid type pulsed nozzle has been used to generate free-jet of the molecule of interest. Drawing D3 shows the nozzle-skimmer assembly of the molecular beam set-up. The pulsed valve has advantage over CW valve, in terms of reduction in duty cycle. Hence, it is possible to use higher stagnation pressure for the given pumping speed of the pump and the nozzle orifice, leading to better characteristics of the molecular beam. The specifications of the nozzle with the controller unit and skimmer are tabulated in Table 2(a) and 2(b), respectively, and the typical characteristics of the nozzle-skimmer assembly are given in Table 2(c).

The nozzle-skimmer assembly has a guide for mounting the nozzle, so that it is in line with the skimmer, when the latter is mounted in its slot. The final alignment of the nozzle and the skimmer is done with the help of a traveling microscope, with an accuracy of better than 20 micron, on both X and Y axes, in the plane of the skimmer orifice. This assembly is subsequently mounted on the mating flange of the expansion chamber, so that it is concentric with both the expansion and the ionization chambers. For this purpose, assembly guides are provided on all the flanges. The con-centricity of the nozzle-skimmer assembly with the chambers is ensured with a He-Ne laser. For pumping purpose, this sub-assembly forms a part of the expansion chamber. The nozzle-skimmer assembly protrudes out into the ionization chamber, and thus, the free-jet is optically accessible via the ionization chamber. In order to carry out studies with the free-jet formed just after the nozzle, three optical ports are available on the nozzle-skimmer assembly. Two of these ports are in line, on the opposite sides, and can be used for exciting the jet molecules, through optical ports on the ionization chamber. The third port is at the right angle to the above ports, and can be used for collecting the fluorescence by the detector mounted on the ionization port in the line with this port.

3.3 Ionization Chamber

The ionization chamber has optical ports in line with the optical ports on the nozzle-skimmer assembly for excitation of molecular jet and for collecting the fluorescence from the

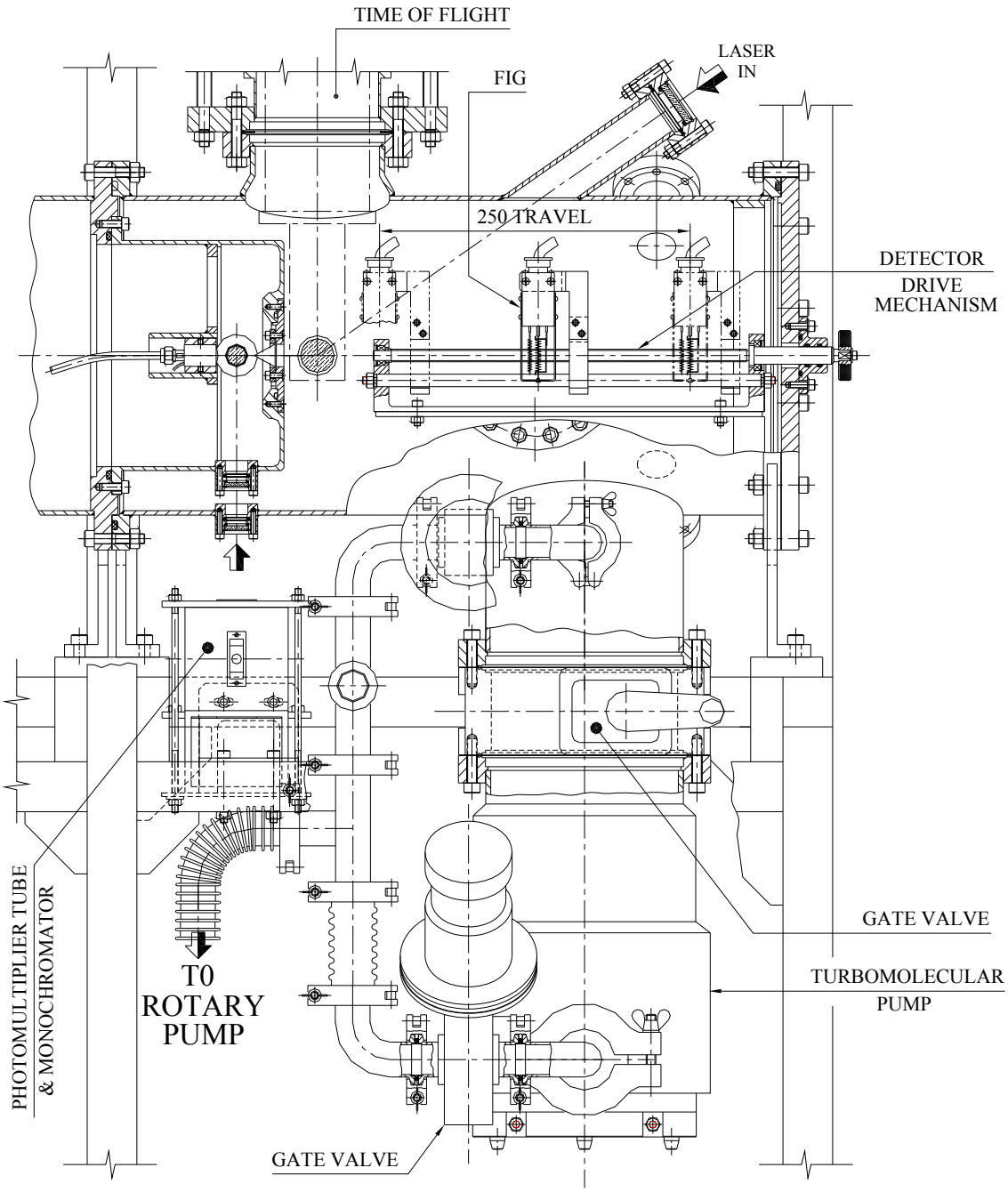

DRAWING D5 : IONISATION CHAMBER WITH PUMP OF MB-REMPI-TOF

excited molecule, as mentioned above. Two optical ports are also provided on the opposite sides of the ionization chamber, for accessing the molecular beam formed by the nozzle-skimmer assembly. It has many other ports, as shown in the drawing D5, for connecting pressure gauge-head, for monitoring vacuum attained, air admittance valve, etc. The fast ionization gauge (FIG) is mounted on the linear motion assembly attached to the free-end flange of the ionization chamber, situated after the ion optics, but in-line with the nozzle-skimmer axis, to monitor the molecular pulse profile and translational energy of the generated molecular beam.

The TOF mass spectrometer assembly is mounted vertically on the side arm, using a 6 inch flexible bellow, which has 6 inch conflate flanges on both the sides, with studs for alignment purpose. The position of the above side-arm on the ionization chamber is such that the ion optics of TOFMS is at right angle to the molecular beam, at the minimum possible distance from the skimmer. The latter is required to obtain a high beam number density at the ionization region of the TOF mass spectrometer.

3.4 Time-of-Flight Mass Spectrometer System

Time-of-flight mass spectrometer (TOFMS) is a simple and efficient mass spectrometer, with almost unity ion transmission. It differs from most of the other mass spectrometers in the sense that it always works in a pulsed mode. It possesses many advantages over the other mass spectrometers. It is relatively less expensive, easy to build, rugged and can be made compact, and does not require rigorous mechanical alignment, or production of stable and uniform electric fields. It consists of three distinct parts, an ion source, an analyzer and a detector. In the first part, the ions are produced, extracted, accelerated and directed into analyzer. A bunch of ions of the species to be analyzed/detected is produced either by electron impact ionization, using a pulsed electron beam, or by photoionization, using a pulsed laser beam, or a flash lamp output, at the region between the repeller plate and the extraction plate. The ions are accelerated to very high energy, and thus reducing the spread in the initial energy of the ions. This is achieved by applying appropriate potential to the acceleration grid with respect to the extraction plate. The kinetic energy of all the ions in a given ion pulse coming out of the ion source is almost the same, and, therefore, the velocity of each ion depends on its mass to charge ratio. The ions are then injected into the analyzer. The analyzer is a field-free drift tube, also called flight tube, wherein the ions travel under field-free conditions, with the velocity obtained in the acceleration region. Here,

the ions are spatially dispersed, depending on their m/z. Lastly, the ions are detected by a dual micro-channel plate (MCP).

In TOFMS, identification of the ions is made on the basis of their flight time from the region of generation to the detector. If the length of the field-free flight tube is very much larger than the acceleration region, then m/z of the ion is related to its flight time 't' by an expression of type,

$$m/z = at^2 + b. \quad (18)$$

The above expression is used for calibrating m/z of ions with respect to their flight times.

In each pulse/cycle, TOF analyzer allows all the ions to pass through, and thus, the complete mass spectrum of the sample can be obtained from a single pulse. Apart from being used as a standalone instrument for analytical work, it is used in many areas of research and development, including process monitoring.

In the present system, the TOFMS assembly, similar to Lubman and Jordan design [16], has been used. The schematic of MB-TOFMS is shown in Fig. 5, and the assembly drawing is shown in drawing D1. The schematic of the TOFMS chamber employed in the present set-up is shown in Fig.6. Fig. 7 shows the schematic of the ion source. All the ion optics plates are 5 cm square in size, and placed 1 cm apart, using insulator beads. The extraction and the accelerator plates have circular aperture of diameter 1 cm at the centre, which are covered by 50 lines/inch stainless steel grids, having 90 % transmission. To direct the ion beam along the axis of the field-free tube, and thus onto the detector, two pairs of plates are placed orthogonal to the detector axis (z axis). These are located above the accelerator plates. This is followed by the field-free drift tube. At the end of this tube, a T-connector, having 6-inch conflate flanges at the ends, is mounted. The other two arms of the T-connector are used for connecting a gate valve and a 250 l/s turbo pump. A dual microchannel plate (MCP) detector is mounted at the other end of the gate valve, for detecting the arriving ions. The above pump is used for pumping the detector region to obtain better vacuum level in the detector region, and the gate valve to isolate the detector from the other assemblies.

3.4.1 Detector System

The detector is a 18 mm active area, dual microchannel plate (MCP), having sub-nanosecond rise time. The detailed schematic is shown in Fig. 8. The mechanical and electrical specifications are given in Table 3. The functioning of MCP was checked by slowly

increasing the voltage applied to its voltage divider (see Fig. 9, for detail), while carefully watching for any undesirable arching and excess noise spikes.

4. Laser and Optics System

The schematic of the integrated system with the required laser system and the control electronics is shown in Fig.3. The laser system comprises an excimer laser (Compex-102, Lambda Physik) and a dye laser (TDL 90, Quantel), pumped by a Nd:YAG laser (YG-981-C, Quantel). The specifications of the laser systems employed are given in Table 4 (a) and (b). The excimer laser is employed as a photolysis laser, for photodissociation of the parent molecule, while the fundamental dye laser output, after doubling, or mixing after doubling, depending on the wavelength required, is used as a probe laser for REMPI technique. In a favourable chemical system, where the chemical species under investigation has absorption at the REMPI line of one of the photofragment, a single-laser system may be employed for both photolysis and probe. In the configuration, where two separate lasers are used for photolysis and probe, these laser beams are used in a counter propagating configuration. Appropriate mirrors/prisms on kinematics mounts are used for the delivery of the laser beams, and lenses are used for focusing the laser beams.

In photodissociation dynamics experiments, the molecular beam is intersected in the extraction region of a Wiley-McLaren type Time-of-Flight mass spectrometer by the photolysis laser beam, propagating perpendicular to both the molecular beams and the TOFMS. The probe (ionization) laser beam counter propagating to the photolysis beam, ionizes the stable products and the radicals produced on photodissociation. These ions are detected by MCP, after their flight through the field free-free drift tube.

5. Control and Electronic System

The schematic of the control electronic system is shown in Fig.10. A digital delay/pulse generator, with pulse resolution of 20 ps, was employed as the master to trigger all the instruments for time synchronization. The detailed specifications of the digital delay/pulse generator employed are given in Table 5. The time delay between the applied trigger pulse to the pulsed valve and the valve opening was obtained by measuring the delay between the trigger pulse and the fast ionization gauge (FIG) signal, employing a digital oscilloscope. This delay is the sum of time required to open the pulsed valve from its trigger input and that for the molecular pulse to reach FIG from its generation, i.e., the nozzle exit. By measuring these time delays for different FIG positions with respect to the skimmer, the

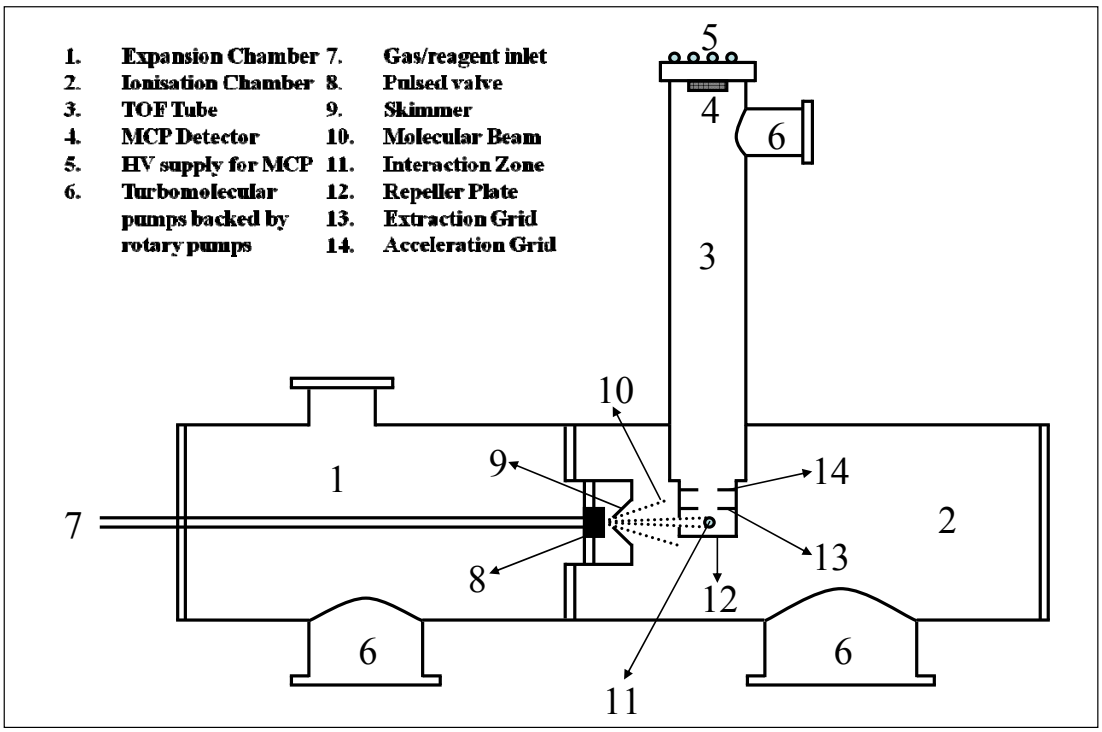

Fig.5: Schematic of MB-TOFMS set-up.

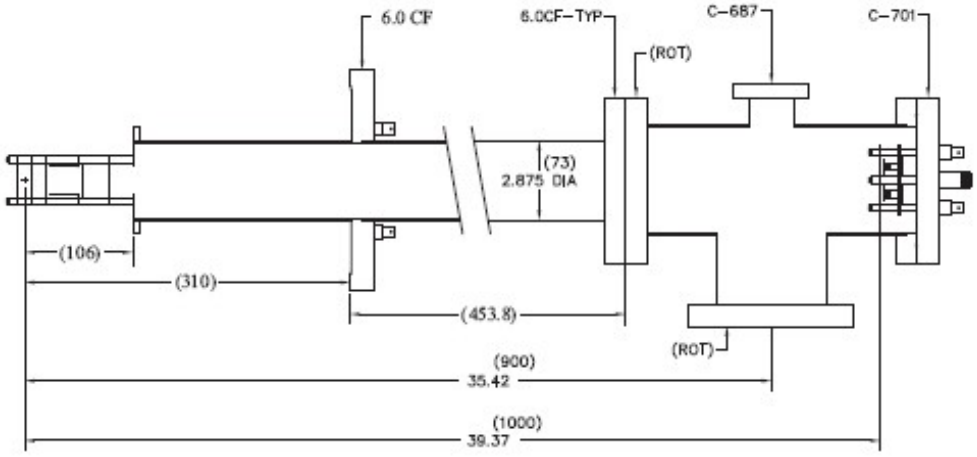

Fig.6: Detailed drawing of the TOFMS chamber.

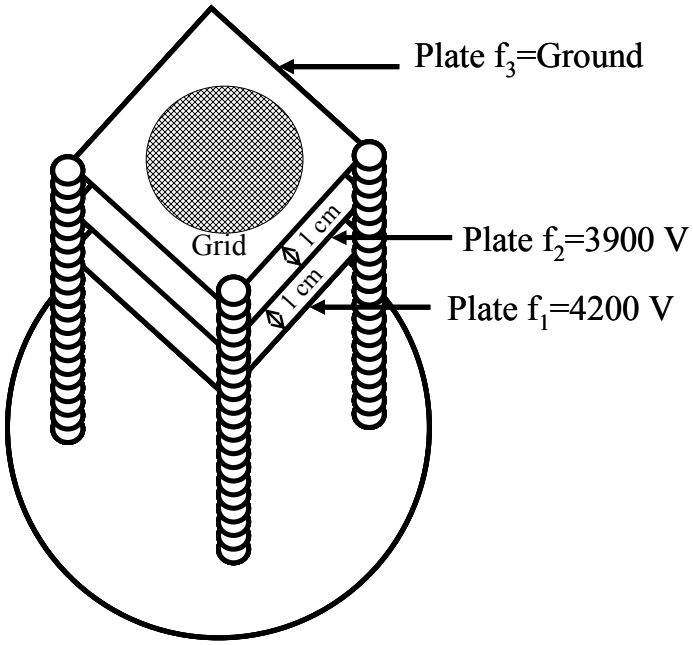

Fig.7: Schematic of the ion optics.

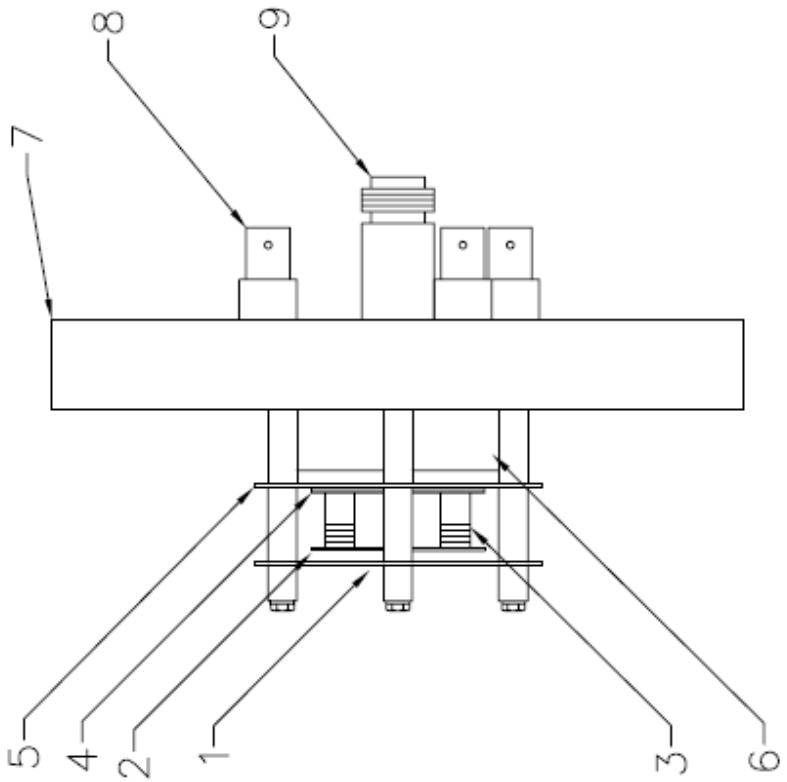

Fig.8: Microchannel plate: 1. Input Grid, 2. Spring Cap, 3. Spring, 4. Channel Plate Stack Assembly, 5. Base Plate, 6. Anode Shield, 7. Detector Flange Assembly, 8. SHV Feedthrough, 9. 50 Ω Feedthrough.

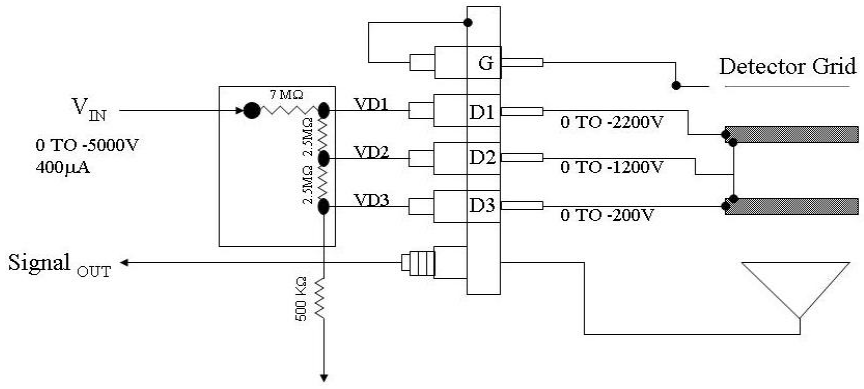

Fig.9: The voltage divider for supplying the requisite power to the MCP.

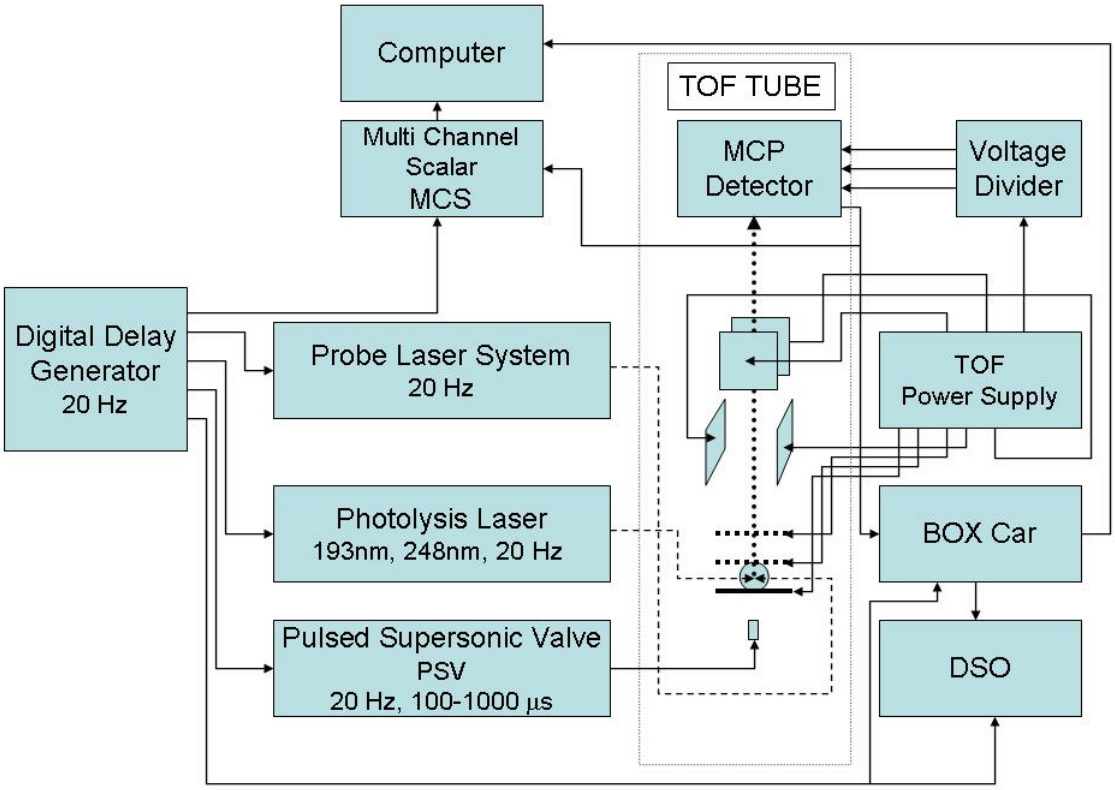

Fig. 10: Schematic of the control electronic system.

Table 3: Mechanical and electrical specifications of the microchannel plate.

S.No.	Parts	Dimension/specification
1	Ground plane grid diameter (input aperature)	0.75 inches
2	Grid transmission	90%
3	Active surface area diameter	0.75 inches
4	Distance from input grid to the face of vacuum flange	1.3 inches
5	Maximum protrusion from the flange face into vacuum system	1.75 inches
6	Minimum tube I.D. for vacuum housing	2.75 inches
7	Maximum voltage across each plate	1000 V
8	Gain per plate at 1000 V	1000

Table 4: Specifications of laser system employed.

a) Excimer Laser (Photolysis laser)

S.NO.	Feature	Optimed Value
1	Energy per pulse (ArF laser)	210 mJ (193 nm), 380 mJ (248 nm)
2	Pulse energy stability $\leq \pm 2\%$	$\leq \pm 2\%$
3.	Pulse width	< 30ns
4.	Temporal jitter	$\leq \pm 5$ ns
5.	Rep. rate	Maximum 50 Hz
6.	Beam divergence	3 x 1 $mrad^2$,
7.	Trigger	Internal and external (TTL)

b) Seeded Nd:YAG pumped dye laser (Ionization laser).

Laser	Feature	Optimed Value
Seeded Nd:YAG	Energy	1000 mJ at 1064 nm
	Pulse width	8 ns
	Line width	0.003 cm^{-1}
	Rep rate	20 Hz
	Temporal jitter	2 ns
Dye laser	Wavelength range	216-850 nm
	Beam divergence	0.5 mrad
	Line width	0.06 cm^{-1}
	Fundamental output Energy	10-25% of Pump energy
	Doubling energy	10-15% of Fundamental output
	Mixing after doubling	15-20% of Doubling output

Table 5: Specifications of delay generator employed in MB-REMPI-TOF set-up.

S.No.	Feature	Properties/parameters	Specifications
1.	Delays	Channels	Four independent delay outputs: A,B,C and D
		Range	0 to 999.999,999,999,995 s
		Resolution	5 ps
		Accuracy	1500 + timebase error x delay
		RMS jitter	60 ps + delay x 10^{-8}
2.	Frequency	Repetition rate	0.001 Hz to 1.000 MHZ
3.	Inputs	External trigger	Impedance : 1 MΩ or 50 Ω
			Threshold : ± 2.56 Vdc
4.	Outputs	Channels	T0, A, B, C, D, AB, -AB, CD and -CD
		Load	50 Ω or high impedance
		Risetime	3 ns
		Type	TTL, ECL, NIM, VAR
5.	Interface	Computer interface	IEEE 488 Standard GPIB

Table 6: Specifications of Fast Ionization Gauge.

S. No.	Feature	Specification
1	Response rise-time	3 μs
2	Useful pressure range	10^{-8}- 10^{-2} torr
3	Sensitivity	1x105 Volt $torr^{-1}$ mA^{-1}
4	RMS noise	20 mV, with Filament on
5	Emission current adjustable	5 μA to 3mA
6	Filament material	Tungsten

Table 7: Specifications of Fast Gated Integrator and averager employed in MB-REMPI-TOF set-up.

S.No.	Feature	Properties	Specifications
1.	Trigger	Internal trigger	0.5 Hz to 20 kHz
		External trigger	1 MΩ input impedance. Trigger threshold adjustable from 0.5 to 2 V
2.	Delay	Delay scale	1 ns to 10 ms
		Insertion delay	25 ns
		Jitter	<20 ps or 0.01 % of full-scale delay, whichever is larger
3.	Gate	Gate Width	1 ns to 15 μs
		Width accuracy	2 ns or 20 % of full scale, whichever is greater
		Minimum width	2 ns, FWHM
4.	Signal	Sensitivity (V_{out}/V_{in})	1V/V to 1V/5 mV
		Offset control	±0.4 VDC
5.	Averaging	Type	Exponential moving average
		Number of samples	Max. 10,000

flow velocity of molecular beam was estimated, and used to obtain the time required for the molecular beam to reach the extraction region of the TOFMS. The detailed specifications of FIG are given in Table 6.

Fast photodiodes (Becker-Hickl Model PDM-400) were used to measure the time delays between the external-trigger inputs and the laser outputs for the photolysis laser (excimer laser) as well as the probe laser (Nd:YAG pumped dye laser). Based on the above measured delays, the trigger pulses of the different instruments were adjusted, so that the photolysis laser pulse and the molecular beam pulse arrive in the interaction zone at the same time, but 100 ns prior to the probe laser pulse.

The ion signal was gate integrated by a boxcar, averaged for 30 laser shots, and fed into an interface (SRS 245), for A/D conversion. The detailed specifications of the Boxcar used are given in Table 7. A PC was used to control the scan of the dye laser via an RS232 interface, and to collect data from SRS 245, through a GPIB interface, using a control and data acquisition program. The laser frequency was calibrated, using an optogalvanic cell (Fe-Ne), with an accuracy of $\pm$ 0.3 cm^{-1}. The spectral resolution of the probe laser is 0.06 cm^{-1}.

A single compact voltage generator, having multiple output voltage ports, was employed to power the TOF ion optics, the deflection plates and the MCP detector. Before applying any voltage to the MCP, it was pumped at a dynamic vacuum of $< 10^{-6}$ torr, for 2-3 days. The grid of the MCP was grounded, while the MCP plates were powered, using a divider box. The voltage applied to the voltage divider box is divided, to provide the requisite voltages to the dual channel MCP detector, as shown in the Fig. 9

6. System Alignment, Standardization and Calibration

The mass spectrometer consists of three regions, the extraction region (E), the acceleration region (A) and the drift region (D). After the ions have passed the three regions, these are collected on an MCP detector, and the resulting signal is collected from the copper anode behind the channel-plates, for further processing.

The initial alignment of the set-up was carried out, using aniline supersonic beam, generated by flowing helium through a bubbler, containing aniline at room temperature, and at a total stagnation pressure of 2.5 bar. To begin with, the molecular beam and the ionization laser were spatially and temporally aligned with the help of the alignment tools. The voltage was applied to the repeller plate only, and the ion signal generated by MCP was fed to an oscilloscope. The ion signal was maximized by aligning ion optics of the TOFMS with

respect to the molecular beam, with the help of the alignment studs, provided on the end-flanges of the bellow. The signal obtained after the above alignment was maximized further, by varying the relative voltages of the deflection plates of the TOFMS. To reduce the spread in the ion signal due to its formation in the finite volume, the space focusing condition is achieved. In the middle of the extraction region, (a region between the repeller and extraction plate of length $2s_0$ = 10 mm, designated as s region), the molecular beam is crossed by the ionizing probe laser. The ions formed are extracted by the applied electric field, E_s, between these plates. Further, the applied electric field, E_d, between extraction and accelerating plates, d region, accelerates these ions in the acceleration region of length, d = 10 mm. This is followed by the electric field-free region, D region, which has length, D = 1147 mm. This region of the spectrometer serves to improve the time resolution and the space focusing of the ions. Each ion formed in the "s" region will leave region "d" with a velocity dependent on its initial position and its m/z ratio, where m and z denote the mass and the charge, respectively, of the ion. The flight time of an ion can be expressed by the relation,

$$t = \frac{v_1 - v_o}{a_1} + \frac{v_2 - v_1}{a_2} + \frac{D}{v_2} \tag{19}$$

where v_o, v_1 and v_2 are the initial velocity of the ion, its velocity at the extractor plane and velocity at the grid plane, respectively, and a_1 and a_2 are the acceleration of the ion between the repeller and the extraction plates, and that between the extraction plate and the acceleration grid, respectively.

In space focusing conditions, the different ions (spatially), with the same m/z ratio, arrive at the detector at the same time. Thus, when the space focusing condition is fulfilled, we can write the total flight time (t) of an ion in the spectrometer as being:

$$t = t_s + t_d + t_D \tag{20}$$

with t_s, t_d and t_D being the flight times corresponding to regions s, d and D, respectively, and having the magnitudes defined by:

$$t_s = 1.02\frac{\sqrt{2m}}{qE_s}\left[\left(\sqrt{U_0 + qsE_s}\right) \pm \sqrt{U_0}\right] \tag{21}$$

$$t_d = 1.02\frac{\sqrt{2m}}{qE_d}\left[\left(\sqrt{U} - \sqrt{U_0 + qsE_s}\right)\right] \tag{22}$$

$$t_D = 1.02\sqrt{2m}\frac{D}{2\sqrt{U}} \tag{23}$$

where the "-" and the "+" signs in eqn.(21) indicate the initial velocity being directed towards and away from the detector, respectively, and U_0 and U are the kinetic energies of the ion in the initial moment and when it leaves the region "d", respectively.

Now, for requirements of space focusing condition, we set $(dt/ds)_{0,s0} = 0$, and using above value for t, we get

$$D = 2s_0 k_0^{\frac{3}{2}}\left(1 - \frac{1}{k_0 + k_0^{\frac{1}{2}}}\frac{d}{s_0}\right) \tag{24}$$

where

$$k_0 = \frac{s_0 E_s + dE_d}{s_0 E_s} \tag{25}$$

For our current experimental set-up the ratio E_s/E_d can be easily calculated, using the above equation by knowing s_0, d and D, which are 5, 10 and 1147 mm, respectively. The only positive real value for the ratio thus calculated was found to be 0.084. The space focusing condition was obtained experimentally, starting with the calculated ratio of E_s/E_d. The ratio was varied by changing E_d at fixed E_s, and at each E_d value, the position of the ionization volume was moved vertically, along the line joining the ionizer and the detector (MCP). The arrival time of the aniline ion was noted at each position, for the particular E_d. The electric field E_d was fixed at the value, where the flight time of the aniline ion was insensitive to the ionization spatial position, and a Gaussian shape of the aniline ion signal, with minimum pulse width, was obtained. The experimental ratio E_s/E_d was 0.077, which is well within 10% of the calculated value.

The observed TOF spectrum of the aniline ion ($C_6H_7N^+$), with the Gaussian shape, is shown in Fig.11, wherein both the $^{12}C_6H_7N^+$ and $^{13}C^{12}C_5H_7N^+$ isotopomers can be seen, with the flight time of 14.08 and 14.15 μs, respectively.

The system was standardized with the aniline beam. The REMPI spectrum of aniline is shown in Fig.12, with the line at 293.77 nm, matching well with the reported value. The aniline ion signal was measured as a function of the laser intensity at resonance wavelength, and found to be quadratic dependent, with a slope = 2.01±0.11 as depicted in Fig.13. This shows that at 293.77 nm, the REMPI is 2+1 type due to two-photon resonant transition, $^1A_1 \rightarrow {}^1B_2$, followed by transition to the ionization continuum by absorption of the third photon.

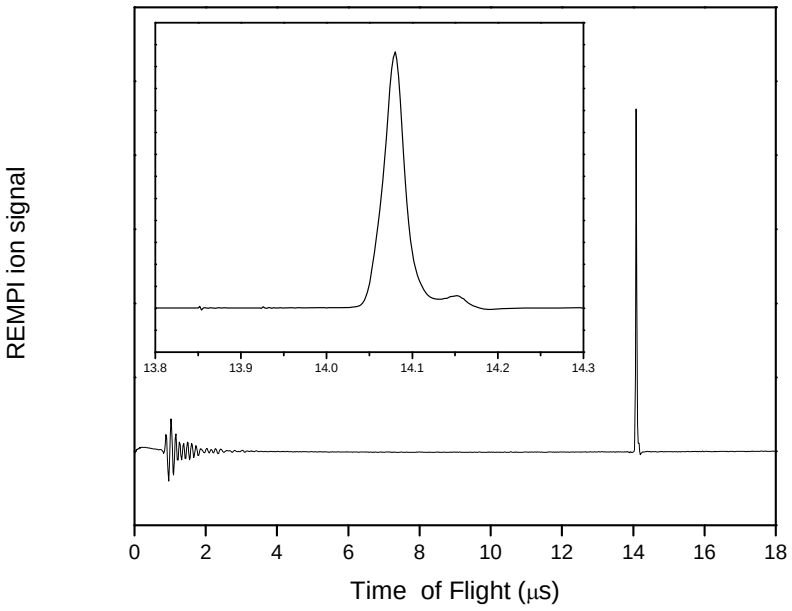

Fig.11: TOF spectra of the aniline ion, and the inset showing the two isotopomer components.

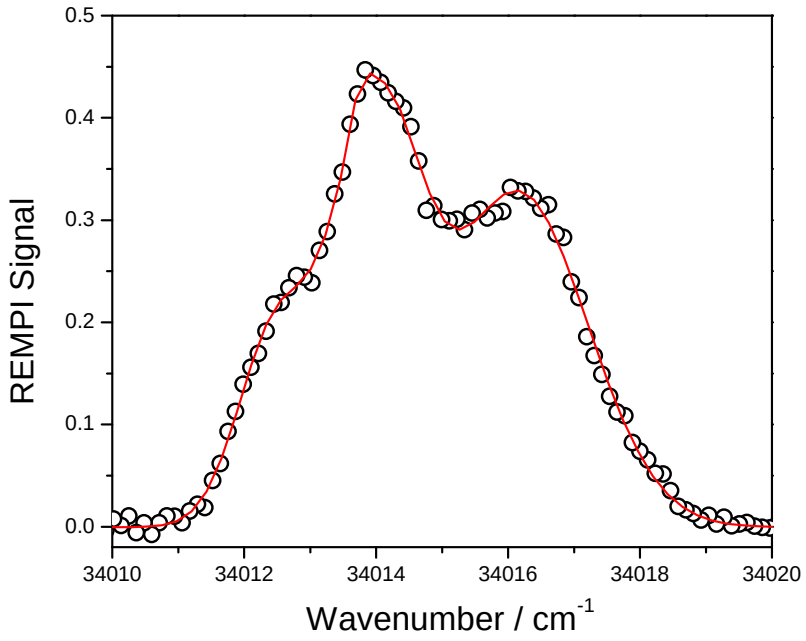

Fig.12: A typical REMPI spectrum of aniline.

6.1 Mass Resolution

Mass resolution is the ability to distinguish adjacent masses, or more accurately, mass-to-charge ratio. In fact, the resolution provides a measure of the highest mass (M) that can be completely separated from its adjacent masses (M±1). Hence, the resolution, R, is scaled to the mass range under consideration, and defined as,

$$R=M/\Delta M \tag{26}$$

where ΔM is the difference in the masses of the species, and M is the average mass of the two ions. For TOF-MS, assuming a single charge on the ion, the mass resolution is defined on the basis of the time-of-flight, t, and peak width (FWHM), Δt, of the ion pulse, by an expression,

$$R = \frac{t}{2\Delta t}. \tag{27}$$

The mass resolution (R) of the set-up was estimated from the arrival time (t) and FWHM (Δt) of aniline ion, using the above relation, to be 400.

6.2 Mass Calibration

The time-of-flight of an ion encompasses contributions from three different regions: the extraction, the acceleration and the field-free drift regions. The ions are generated by absorption of photons, at the centre of the ionization region, defined by the repeller and the extraction plates. These ions experience two accelerating fields, the repeller-extraction and the extraction-acceleration regions. This is followed by the field-free drift region of length, D. The eqn. (20) is used to estimate an approximate flight time of ions. However, for calibration of TOFMS, the flight time of several known ions, like Br^+, Cl^+, CH_3Br^+, $aniline^+$, $CHBr^+$, Br_2^+, Cl_2^+, etc., was measured. A plot of m/z versus the flight time (t), Fig.13, was fitted with the empirical equation (18). From the fitting parameters ‘a’ and ‘b’, the flight time of many other ions were estimated, and found to be in the good agreement with the measured values.

6.3 Sensitivity and Detection Limit

Sensitivity, in a broader sense, is defined as the ratio of change in the signal level of the instrument to the change in the analyte concentration. In practical sense, the analyte concentration, for which the signal-to-noise ratio is 3, is taken as the detection limit of the

instrument in terms of the analyte concentration. In the present set-up, with 3000 V applied to the divider of MCP, a RMS noise of 2 mV was observed. An analyte concentration capable of generating a signal of 6 mV can be considered as the detection limit of the set-up. The concentration of the analyte, corresponding to the above signal strength, can be back calculated.

In (2+1) REMPI process, assuming the final pumping to the ionization continuum is saturated at the laser intensity employed, and hence intensity independent, the number of ions produced, N_i, is expressed as,

$$N_i = n_0 \sigma_{abs} I^2 \tau V_{int} \quad (28)$$

where n_0 is the number density of the neutral chemical species under investigation, σ_{abs} is two-photon absorption cross section, I and τ are the intensity and the pulse width of the laser, respectively, and V_{int} is the interaction volume of the molecular and the laser beams. Assuming that all the ions generated by the laser pulse of width, τ, reach the detector of gain, G, and terminated by a resistance, R = 50 Ω, the output voltage, S, of the detector is

$$S = N_i G R/ \tau. \text{ x } 1.6 \text{ x} 10^{-19} \quad (29)$$

Combining equations, (28) and (29), we get

$$S = n_0 \sigma_{abs} I^2 \ V_{int} G R \text{ x } 1.6 \text{ x} 10^{-19}. \quad (30)$$

In the present set-up, a 10 ns pulse of Nd:YAG pumped dye laser, on frequency mixing after doubling, is employed for photo-ionization. The typical laser pulse used has energy of 3 mJ and the beam size of 2 mm. The interaction volume, defined by the spatial overlap of the laser and the molecular beams has a typical value of 0.025 cm^3. The gain of the detector employed is 10^8 at a typical voltage of 3000 V. To calculate I, in terms of photons cm^{-2} sec^{-1}, from the laser pulse energy, the wavelength of photon is considered to be 300 nm. Assuming a typical value of two-photon absorption cross section, σ_{abs}, to be 10^{-50} cm^4sec $molecule^{-1}$ $photon^{-1}$, the above relation estimates the number of analyte molecules in the interaction volume to be 6.2x 10^6, or 2.5x10^8 molecules cm^{-3}, to obtain a signal of 6 mV. Hence, we estimate theoretically a detection limit of 2.5x10^8 molecules cm^{-3}.

Experimentally, detection limit of the system is measured for both the resonant and the non-resonant photoionization processes. Fig.15 is a typical TOF mass spectrum of the

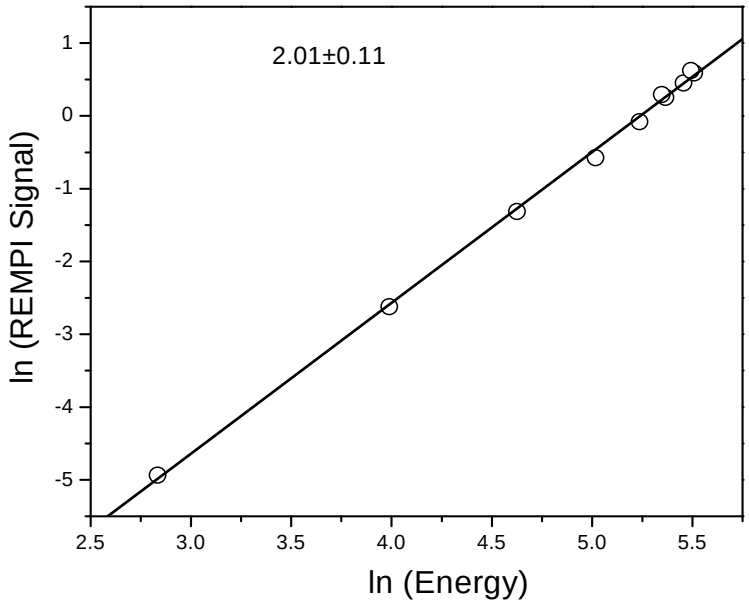

Fig.13: Power dependence of REMPI signal of aniline.

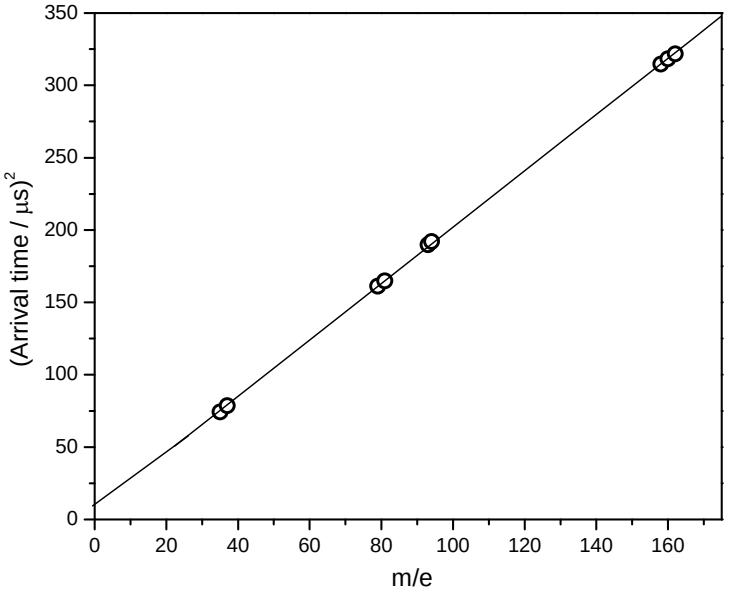

Fig.14: A plot of square of the arrival time against the m/z of the ions in REMPI-TOFMS.

residual gases at a background pressure of 10^{-7} torr, formed due to non-resonant ionization. The peaks can be assigned to the ionization products of the pump oil. At 10^{-7} torr, the maximum number density of the residual gas molecules is 10^9 molecules cm^{-3}. This confirms very low detection limit of the set-up, as estimated from the calculation shown above.

The detection limit was also obtained from the aniline REMPI spectrum. For aniline beam, formed by seeding the saturated vapour pressure of aniline, 0.67 torr, in 2.5 atmosphere of helium at 25^0C, a signal of 15 V was obtained by photoionizing aniline with a two-photon resonant transition at 293.77 nm, which is at the peak of the origin of the $^1A_1 \rightarrow {}^1B_2$ transition. In order to obtain the detection limit for aniline, from the above data, the number density of aniline at the ionization region has to be estimated. The number density of aniline under the above conditions obtained from eqn. (17) is 1.14×10^{10} molecules cm^{-3}, and, therefore, the number of molecules in the interaction is 2.85×10^8. Assuming linearity of the REMPI signal to the number density of species under consideration, a signal of 6 mV is expected from 1.10×10^5 molecules in the interaction volume, which implies a number density of 4.56×10^6 aniline molecules cm^{-3}. The use of preamplifier and multi-scalar analyzer further improves the detection limit by an order of magnitude.

7. Photodissociation Dynamics Studies Employing MB-REMPI-TOFMS

Once the MB-REMPI-TOFMS was standardized, we embarked on investigation of photodissociation dynamics of bromoform, to explore capability and versatility of the system developed. It has been estimated by Sturges and co-workers [17] that bromoform contributes about 3% of the total bromine measured in both the troposphere and the lower stratosphere. However, it accounts for more than 9% of the reactive bromine in stratosphere, due to its high absorption cross section. Therefore, from the point of view of ozone destruction in the stratosphere, the photodissociation of $CHBr_3$ has received a lot of attention. The following are some of the important dissociation pathways based on energetics,

$$CHBr_3 \rightarrow CBr_2 + HBr \qquad 245 \text{ kJ/mol}, \qquad (31)$$

$$\rightarrow CHBr_2 + Br \qquad 258 \text{ kJ/mol}, \qquad (32)$$

$$\rightarrow CHBr + Br_2 \qquad 349 \text{ kJ/mol}, \qquad (33)$$

$$\rightarrow CBr + HBr + Br \qquad 530 \text{ kJ/mol}. \qquad (34)$$

Further, in the reactions (32) and (34), Br atom may be formed in the ground state, $Br_{3/2}=(4P^5\ {}^2P_{3/2})$, or the spin-orbit excited state, $Br_{1/2}=(4P^5\ {}^2P_{1/2})$, hereafter, referred to as Br and Br*,

respectively. It is well known that in the photolysis of bromoform [18], Br atom elimination is a major channel. Hence, the present study was directed to measure Br/Br* ratio in the photodissociation of bromoform at ~ 234 nm. For this purpose, molecular beam of $CHBr_3$ was generated by flowing helium through a bubbler, containing $CHBr_3$ at room temperature at total stagnation pressure of 1.5 bar. The photodissociation dynamics experiments were performed by combining REMPI and TOF mass spectrometer to state-selectively monitor Br and Br* atoms. The (2+1) REMPI transitions of Br and Br* atoms, in the wavelength region of 230-235 nm, were used to probe Br and Br* atoms. The laser pulses were generated from a Quantel dye laser, TDL 90, using rhodamine 101 (LC 6400) dye solution in methanol, pumped by a Quantel seeded Nd:YAG laser, YG-981-C-20. The fundamental dye laser output was frequency-doubled in a KDP crystal, and mixed with the fundamental output of the Nd:YAG laser, to obtain an output in the range 230-235 nm. The above laser output was separated from the rest of laser beams, using four Pellin-Broca prisms. In all the experiments reported in this report, the same laser beam was employed as a pump and a probe, i.e., for both photodissociation of the parent molecule and ionization of the photoproducts Br and Br* atoms. The laser beam was focused by a lens of 280 mm focal length, and the distance of the lens from the centre of the molecular beam axis was varied, to obtain the best ratio of on- and off- resonance signals. Fig.16 shows a typical TOF spectrum of the Br product from $CHBr_3$. The peaks in the TOF spectrum are due to two isotopes of Br, at 79 and 81 mass units.

The REMPI spectrum was obtained by recording the integrated TOF signal (with a gate covering both m/z=79 and m/z=81 signal), as a function of the probe laser wavelength. The typical spectrum obtained is shown in Fig.17. The assignments to the resonance transitions obtained in the present study are given in the Table 8, which match very well with the values reported in the literature.

The dependence of the REMPI signal of Br atoms on the probe laser intensity, in one-colour experiments, was investigated. The log-log plot is linear in the range of intensity employed, with a slope of 3.0±0.2, as shown in Fig.18.

The relative quantum yields of Br and Br* were extracted from the relative integrated signal intensities in the TOF spectrum.

$$\frac{N_{Br^*}}{N_{Br}} = R\,\frac{I_{Br^*}}{I_{Br}} \tag{35}$$

$$\Phi_{Br} = \frac{N_{Br}}{N_{Br} + N_{Br^*}} = \left(1 + N_{Br^*} \Big/ N_{Br}\right) - 1 \tag{36}$$

$$\Phi_{Br^*} = \frac{N_{Br^*}}{N_{Br} + N_{Br^*}} = \left(1 + N_{Br} \Big/ N_{Br^*}\right)^{-1} \tag{37}$$

where N_X and I_X are the number and the integrated signal, respectively, for the species indicated in the subscript. The parameter R is the ratio of the oscillator strengths for the corresponding transitions of Br and Br*. The ratio of the integrated areas for the two-photon transitions of Br* and Br was found to be 3.1 (depicted in Fig.19), which estimates Br* ($^2P_{1/2}$)/Br ($^2P_{3/2}$) ratio to be 1.4, using R=0.46 [19]. Similar value (1.38) for the relative yield of Br* ($^2P_{1/2}$)/Br ($^2P_{3/2}$) was observed in photodissociation of BrCl at 235 nm [20].

8. Summary

We have developed a versatile MB-REMPI-TOFMS system for investigation of photodissociation dynamics of isolated molecules. We have kept provision for LIF detection also. Generating a molecular beam of aniline by seeding 1% aniline in helium, and recording its REMPI-TOF spectrum at 293.77 nm, the two important parameters of the system namely, the resolution and the detection limit, have been determined. For the present configuration, using one metre long flight tube, the resolution has been found to be about 400, and detection limit is better than 10^6 species per cm^3. After standardization, the set-up has been employed to study the photodissociation dynamics of bromoform. On photodissociation, the bromine atoms are generated, both in the ground and the spin-orbit excited states, which are probed in the region of 233 - 235 nm, with a spectral resolution of 0.06 cm^{-1}. The probe radiation is generated by frequency-doubling SLM-Nd:YAG pumped dye laser fundamental output, followed by mixing it with the fundamental frequency of Nd:YAG laser.

Acknowledgements

The authors gratefully acknowledge Dr. S.K. Sarkar, Head, Radiation & Photochemistry Division, Dr. T. Mukherjee, Director, Chemistry Group, and Mr. R.L. Suthar , Head, Centre for Design and & Manufacture, for their keen interest and support. The support from the

technical and auxiliary staff of both Radiation & Photochemistry Division and Centre for Design and & Manufacture is duly acknowledged.

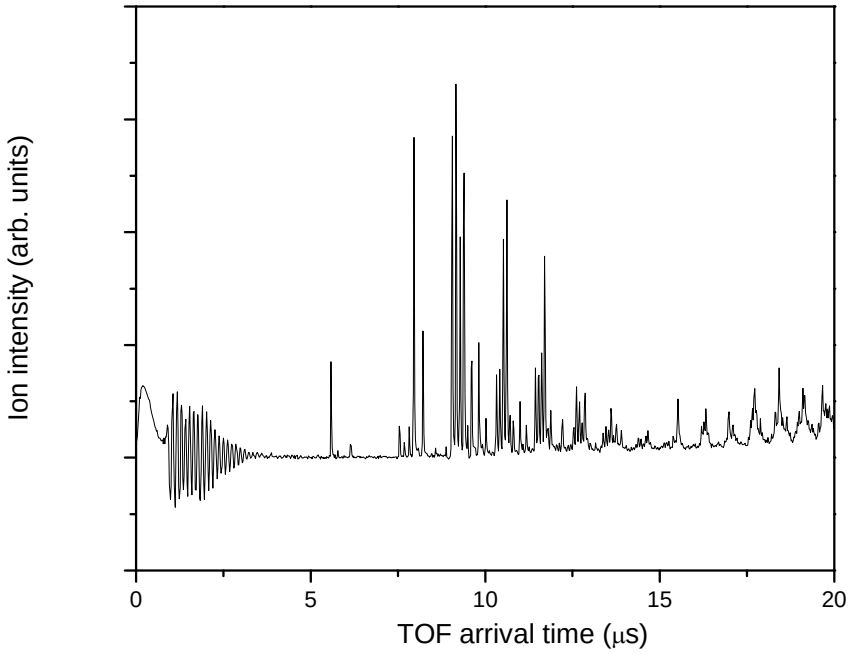

Fig.15: A TOF mass spectrum of the residual gases at the background pressure of 10^{-7} torr.

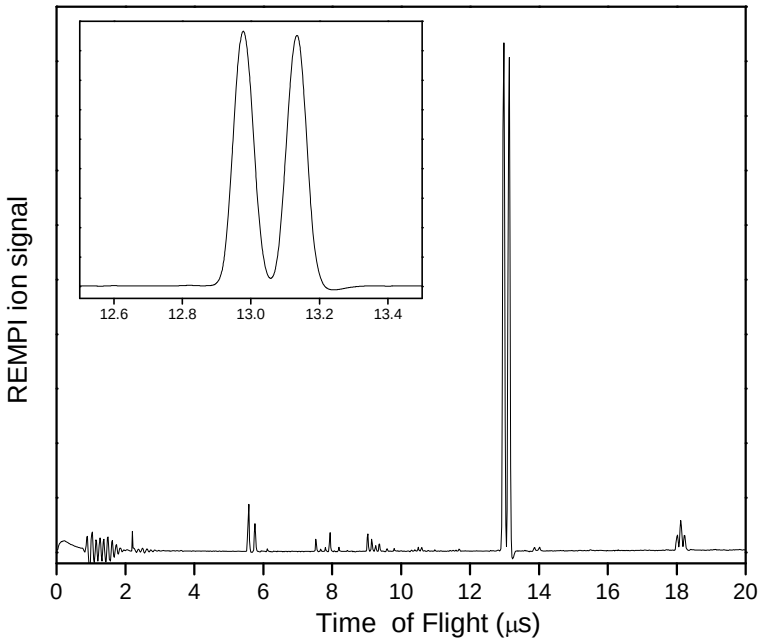

Fig.16: Typical TOF spectra of Br produced from photolysis of $CHBr_3$.

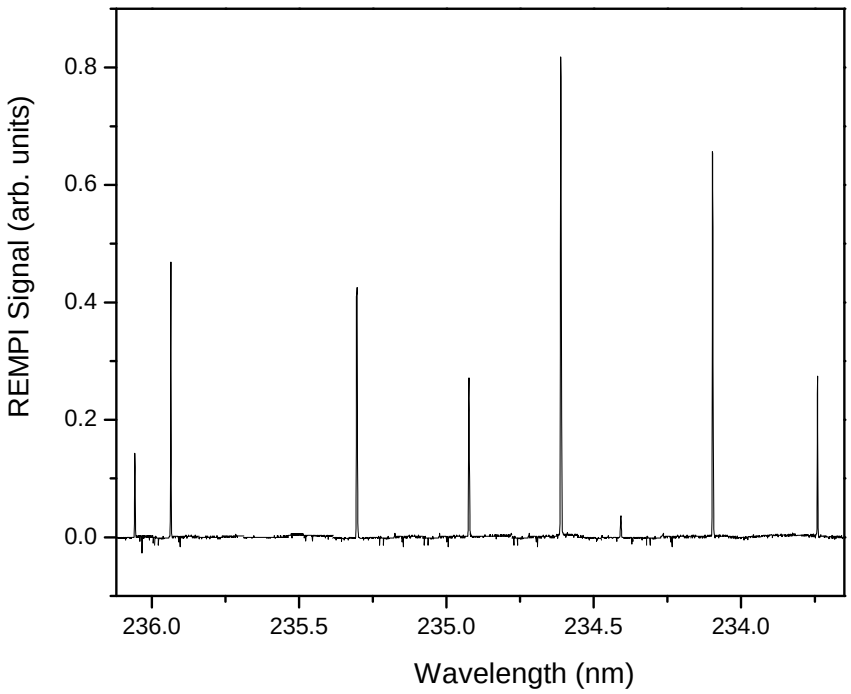

Fig.17: The REMPI spectrum of Br produced from $CHBr_3$.

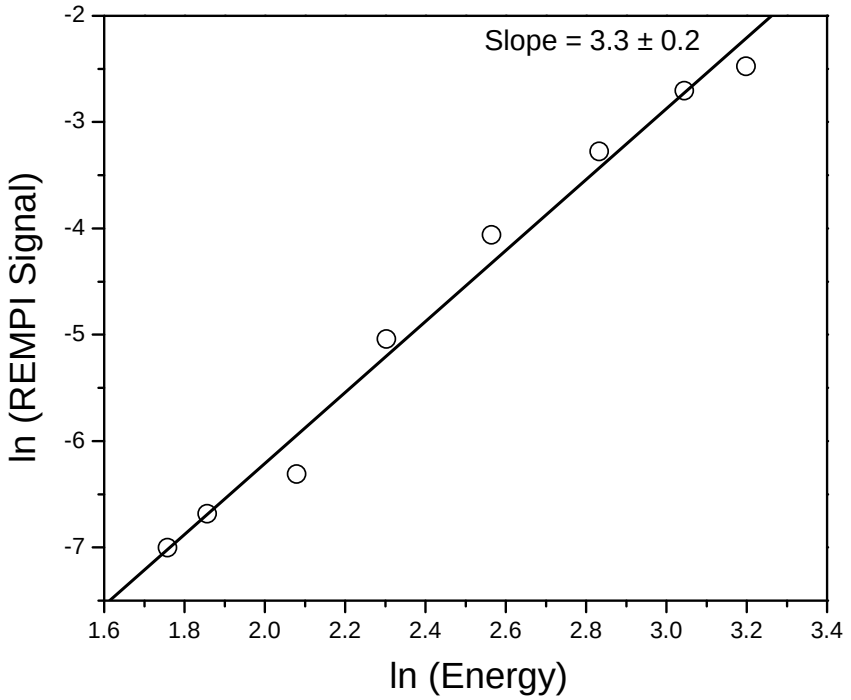

Fig.18: Power dependence of the REMPI signal of Br atoms in one-colour experiment.

Table 8: REMPI transitions of Br.

Peak No	Experimental wavelength	Literature wavelength	Two photon Transition From 4p
1	233.74	233.70	$6p\,^4P_{3/2} \leftarrow 4p\,^2P_{3/2}$
2	234.09	234.04	$6p\,^2S_{1/2} \leftarrow 4p\,^2P_{1/2}$
3	234.41	234.35	$6p\,^2D_{5/2} \leftarrow 4p\,^2P_{1/2}$
4	234.61	234.57	$6p\,^4S_{3/2} \leftarrow 4p\,^2P_{1/2}$
5	234.92	234.86	$6p\,^2D_{3/2} \leftarrow 4p\,^2P_{1/2}$
6	235.30	235.32	$5p\,^2F_{5/2} \leftarrow 4p\,^2P_{1/2}$
7	235.93	235.66	$5p'\,^2P_{1/2} \leftarrow 4p\,^2P_{1/2}$
8	236.00	235.87	$5p'\,^2P_{3/2} \leftarrow 4p\,^2P_{1/2}$

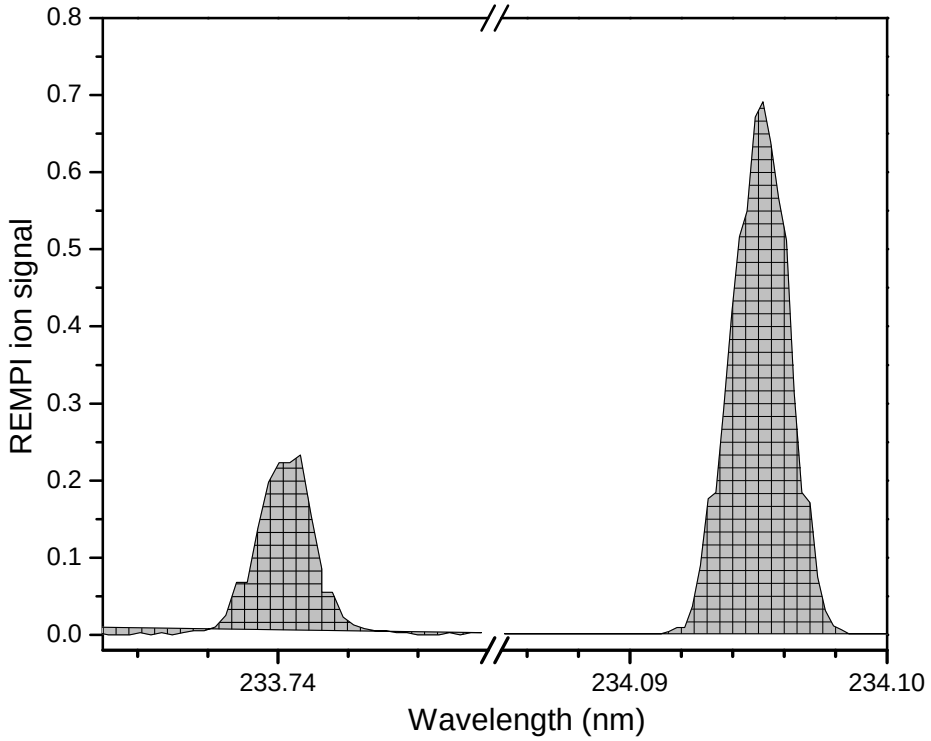

Fig.19: The spectral profiles of REMPI signals of Br and Br*

References

1. W.S. McGiven, R. Li, P. Zou, S.W. North, J. Chem. Phys. 111 (1999) 5771.
2. P.K. Chakraborti, R. Talukdar, P.N. Bajaj, A. Joshi, V.B. Kartha, Chem: Phys. 95 (1985) 145.
3. P.D. Naik, Awadhesh Kumar, H.P. Upadhyaya, P.N. Bajaj, S.K. Sarkar, Lasers in Chemistry, Vol.1, Ed. M. Lackner, Wiley-VCH Verlag GmbH (2008), p.463.
4. Sumana Sengupta, Yogesh Indulkar, Awadhesh Kumar, Suresh Dhanya, P.D. Naik, P.N. Bajaj, J. Phys. Chem. *A* 112 (2008) 12572.
5. Awadhesh Kumar, Hari P. Upadhyaya, P.D. Naik, J. P. Mittal,. J. Phys. Chem. A 106 (2002) 11847.

6 Hari P. Upadhyaya, Awadhesh Kumar, P.D. Naik, J. Chem. Phys. 118 (2003) 2590.

7 P.D. Naik, Hari P. Upadhyaya, Awadhesh Kumar, A.V. Sapre, J. P. Mittal, J. Photochem & Photobiol. C: Photochemistry Rev. 28 (2002) 1.

8. W.C. Wiley, I.H. McLaren, Rev. Sci. Instrum. 26 (1955) 1150.
9. R. Compargue, A. Labehot, J.C. Lemonnier, D. Marette, J. Pebay, 5th Symp. Int. Jets Mol. Abstr., 1975, Nice, France.
10. J.B. Anderson, Molecular Beams and Low Density Gas Dynamic, Vol. 4, Ed. P.P. Wegner, (Dekker, New York, 1974), Chap. 1.
11. P.N. Bajaj, P.K. Chakraborti, Chem: Phys. 104 (1986) 41.
12. J.B. Anderson, J.B. Fenn, Phys. Fluids 6 (1967) 780.
13. H. Ashkenas, F.S. Sherman in "Rarefied Gas Dynamics, Vol. 2, Ed. J.H. deLeeuw (Academic Press, New York, 1966) P.84.
14. A. Kantrowitz, J. grey: Rev. Sci. Instrum. 22 (1951) 328.
15. J.B. Anderson, R.P. Andres, J.B. Fenn, Adv. Chem. Phys. 10 (1968) 275.
16. D.M. Lubman, R.M. Jordan, Rev. Sci. Instrum. 56 (1985) 373.
17. W.T. Sturges, D.E. Oram, L.J. Carpenter, S.A. Penkett, A. Engel, Geophys. Res. Lett. 27 (2000) 2081.
18. D. Xu, J.S. Francisco, J. Huang, W.M. Jackson, J. Chem. Phys. 117 (2002) 2578.
19. P. Zou, W.S. McGiven, S.W. North, Phys. Chem. Chem. Phys. 17 (2000) 3785.
20. M.-S. Park, Y.-J. Jung, S.-H. Lee, D.-C. Kim, K.-H. jung, Chem. Phys. Lett. 322 (2000) 429.